

Impacts of reductions in anthropogenic aerosols and greenhouse gases toward carbon neutrality on dust pollution over the Northern Hemisphere dust belt

Shicheng Yan^{1,2}, Yang Yang^{1,2*}, Lili Ren³, Hailong Wang⁴, Pinya Wang², Lei Chen²,
Jianbin Jin^{1,2}, Hong Liao^{1,2}

¹State Key Laboratory of Climate System Prediction and Risk Management/Jiangsu Key Laboratory of Atmospheric Environment Monitoring and Pollution Control/Jiangsu Collaborative Innovation Center of Atmospheric Environment and Equipment Technology/Joint International Research Laboratory of Climate and Environment Change, Nanjing University of Information Science and Technology, Nanjing, Jiangsu, China

²School of Environmental Science and Engineering, Nanjing University of Information Science and Technology, Nanjing, Jiangsu, China

³School of Environment and Ecology, Jiangsu Open University, Nanjing, Jiangsu, China

⁴Atmospheric, Climate, and Earth Sciences Division, Pacific Northwest National

Laboratory, Richland, W.

* Correspondence to Yang Yang (yang.yang@nuist.edu.cn)

26 **Abstract**

27 To mitigate future global warming, many countries have implemented rigorous
28 climate policies for carbon neutrality. Given some shared emission sources with
29 greenhouse gases (GHGs), aerosol particles and their precursor emissions are expected
30 to be reduced as the consequences of global efforts in climate mitigation and
31 environmental improvement, potentially inducing complex climate feedbacks.
32 However, a clear understanding of the individual effects of anthropogenic aerosols and
33 GHGs on natural dust concentrations has not yet emerged, especially in the carbon
34 neutral scenario. Here, we assess the large-scale impacts of reductions in anthropogenic
35 GHGs and aerosol under a carbon neutral scenario in 2060 on natural dust emissions
36 and concentrations over the low- to mid-latitudes in the Northern Hemisphere using the
37 fully coupled Community Earth System Model. Our findings demonstrate a decline in
38 atmospheric dust loading toward carbon neutrality (SSP1-1.9) relative to the high fossil
39 fuel scenario (SSP5-8.5). Mechanistic analysis reveals counteracting modulation
40 mechanisms: (i) Reductions in aerosols amplify surface downwelling shortwave
41 radiation, convection and wind speed, thereby promoting dust emissions by 6–12% and
42 concentrations by 4–20% over North Africa, the Central Asia Desert and East Asia; (ii)
43 GHGs reductions diminish the land-ocean thermal contrast and wind speed, suppressing
44 dust emissions by 6–15% and concentrations by 8–20% mainly over the Central Asia
45 Desert and North Africa. The latter drives the future dust responses. These results
46 highlight that carbon neutral strategies not only achieve climate mitigation goals and
47 air quality improvements, but also generate synergistic benefits through dust pollution
48 suppression.

49

50 **1. Introduction**

51 Dust aerosols are a crucial component of the Earth-atmosphere system, exerting
52 multifaceted influences on environment and climate (Chen et al., 2024; Hu et al., 2023).
53 They play a significant role in modulating the Earth's radiation budget via aerosol-cloud
54 and aerosol-radiation interactions. Dust aerosols absorb longwave radiation and scatter
55 shortwave radiation, thereby influencing atmospheric radiative balance and surface
56 energy fluxes (Kok et al., 2017, 2023; Liu et al., 2021). Additionally, dust aerosols act
57 as cloud condensation nuclei, modifying cloud microphysical properties and
58 subsequently affecting cloud development and precipitation patterns (Min et al., 2009;
59 Yuan et al., 2021; Zhang et al., 2021). In addition, mineral dust ~~undergoes long range
60 atmospheric transport, affecting biogeochemical processes in transports iron to marine
61 ecosystems through iron deposition (Jickells et al., 2005), which stimulates, stimulating
62 phytoplankton biomass production growth and amplifies the biological enhancing
63 carbon fixation efficiency (Jickells et al., 2005; Pabortsava et al., 2017)~~. Furthermore,
64 dust can reduce visibility, degrade air quality and have important impacts on public
65 health, particularly in arid and semiarid regions (Fussell et al., 2021; Goudie et al., 2014;
66 Li et al., 2024; Roy et al., 2023). These health risks are extended beyond proximal desert
67 margins to distal urban centers by intercontinental transport mechanisms (Griffin et al.,
68 2007; Meng et al., 2023).

69 The global primary sources of dust emissions are located in the arid zones of the
70 low- to mid-latitudes in the Northern Hemisphere, with core areas concentrated in the
71 Sahara Desert of North Africa, the Central Asia Desert, Arabian Desert, Taklamakan
72 Desert, and Gobi Desert of East Asia, which is often called the dust belt (Prospero et
73 al., 2002; Shao et al., 2011). Specifically, the North African desert, as the world's largest
74 dust source, injects approximately 1.0-1.5 billion tons of dust aerosols annually into the
75 atmosphere, accounting for 50%-65% of the global total dust emissions (Tanaka et al.,
76 2006; Ginoux et al., 2004). Meanwhile, Asian dust sources contribute 30%-40% of the
77 global dust flux and are identified as the second-largest emission center (Kok et al.,
78 2021).

79 Dust emission is influenced by climate change, determined by a combination of
80 natural and anthropogenic factors, including greenhouse gases (GHGs) concentrations,
81 aerosol loading, and land use, with anthropogenic contributions exhibiting increasing
82 influence in the post-industrial era (Gui et al., 2022; Tegen et al., 2004). Variations in

83 GHGs concentrations further regulate dust transport through large-scale atmospheric
84 teleconnections. Elevated GHGs levels amplified the North Atlantic Oscillation (NAO)
85 (Kuzmina et al., 2005), which changed atmospheric circulation patterns and enhanced
86 dust advection to South Asia (Banerjee et al., 2021). The strengthened West African
87 monsoon under warming conditions was found to amplify dust emissions (Wubben et
88 al., 2024). In the arid and semi-arid regions of North and Central Asia, surface warming
89 enhanced atmospheric instability, thereby intensifying vertical convective motions and
90 significantly increasing dust emission fluxes (Zhou et al., 2023). Anthropogenic
91 aerosols are recognized as an important forcing factor in global and regional climate
92 systems (Ramanathan et al., 2001; Myhre et al., 2017). Analyses of observations from
93 1979 to 2013 showed that anthropogenic sulfate aerosols over the Asian monsoon
94 region suppressed dust emissions in East Asia by altering atmospheric dynamics (Xie
95 et al., 2025). Specifically, sulfate-induced shifts in the Asian westerly jet enhanced
96 precipitation and reduced surface wind speeds across arid and semi-arid source regions,
97 thereby limiting dust mobilization. Model simulations illustrated that the combined
98 reduction of carbonaceous aerosols (black carbon and organic carbon) and increased
99 sulfate emissions in South Asia synergistically caused atmospheric cooling over
100 continental regions, which attenuated the zonal thermal gradient, resulting in a
101 weakening of the Indian summer monsoon circulation (Das et al., 2020). Concurrently,
102 this altered atmospheric circulation suppressed dust emissions from the Arabian
103 Peninsula and inhibited dust transport across the Arabian Sea. Observational and
104 reanalysis data from the COVID-19 pandemic period revealed that anthropogenic
105 aerosol emission reductions over the Indian subcontinent amplified the Indian summer
106 monsoon intensity and triggered anomalous convective activity over the tropical Indian
107 Ocean, which increased surface wind speeds and enhanced dust lifting over the Arabian
108 Peninsula (Francis et al., 2022). Modeling studies have found that reductions in
109 anthropogenic aerosol emissions along the West African coast led to a decrease in
110 aerosol loading, triggering a northward shift of the monsoonal precipitation belt. This
111 meridional displacement subsequently enhanced surface wind speeds over the Saharan
112 arid zone, thereby increasing mineral dust emission fluxes through intensified wind
113 erosion processes (Menut et al., 2019).

114 Under future climate change, dust distribution will vary depending on the
115 projected scenarios. Using the Coupled Model Intercomparison Project Phase 5
116 (CMIP5) multi-model simulations, Singh et al. (2017) showed a 30% increase in

117 regional dust loading over the South Asian monsoon region by the end of the 21st
118 century (2076-2100) relative to 1976-2000 under the RCP8.5 scenario. Zhao et al.
119 (2023) analyzed the multi-model results under four Shared Socioeconomic Pathways
120 (SSPs) from the Coupled Model Intercomparison Project Phase 6 (CMIP6) and found
121 that global dust loading was expected to increase by 2.0-12.5% by the end of the 21st
122 century in most future scenarios, except for SSP3-7.0, which shows a slight decline.
123 Liu et al. (2024) estimated a substantial increase in dust mass loading over North Africa
124 during 2081-2100 under SSP1-2.6, SSP2-4.5, SSP3-7.0, and SSP5-8.5 scenarios from
125 bias-corrected CMIP6 models. Woodward et al. (2005) showed through HadCM3-
126 coupled model experiments that the annual mean global dust burden would rise by
127 225%, from the 2000 baseline ($4 \times 10^4 \text{ mg m}^{-2}$) to $1.3 \times 10^5 \text{ mg m}^{-2}$ by 2100, under a
128 medium-emission scenario, attributed to desertification and climate change. Gomez et
129 al. (2023) projected that rising CO₂ concentrations would elevate global mean PM_{2.5}
130 levels, partly driven by intensified dust aerosol emissions attributable to a strengthened
131 West African monsoon. Akinsanola et al. (2025) found that African easterly wave
132 activity was projected to undergo a robust intensification across the Sahel region under
133 both SSP2-4.5 and SSP5-8.5 scenarios by the end of the 21st century, with profound
134 implications for Saharan dust emission and transport. These studies mainly focus on
135 investigating dust variations under different Shared Socioeconomic Pathways, thereby
136 examining only the combined effects of anthropogenic aerosols and GHGs. However,
137 relatively little attention has been paid to quantifying the individual contributions of
138 anthropogenic aerosols and GHGs changes to the changing dust concentrations in the
139 future, especially in the carbon-neutral scenario.

140 The future climate changes toward carbon neutrality would also affect dust
141 aerosols, which remains largely unknown. Many countries have committed to achieve
142 carbon neutrality by the middle of the 21st century to limit global temperature rise to
143 below 2°C or even 1.5°C by the end of the 21st century. The pursuit of carbon neutrality
144 will reshape anthropogenic emissions associated with climate and environmental
145 policies, driving changes in atmospheric composition and radiative forcing (Wang et
146 al., 2023; Yang et al., 2023). As nations reduce GHGs and aerosol emissions to mitigate
147 global warming, these shifts are expected to induce complex climate influences. Studies
148 have suggested that anthropogenic aerosol reductions could enhance surface
149 downwelling shortwave radiation, elevate near-surface temperatures, and increase wind
150 speed (Lei et al., 2023; Ren et al., 2024). Projections indicated that by the end of the

151 21st century, interannual precipitation variability will intensify by 3.9% and 5.3% under
152 1.5°C and 2.0°C warming scenarios, respectively (Chen et al., 2020). Consequently, the
153 implementation of carbon neutrality policies is likely to modify the current climate state
154 and affect various meteorological variables (Seager et al., 2019; Lee et al., 2013), which
155 are expected to influence dust mobilization.

156 In the carbon-neutral future, reductions in GHGs and aerosols can change climate
157 and meteorological factors, which further affect dust emissions and concentrations.
158 However, existing studies typically focus on dust flux responses to climate change
159 under future scenarios, thereby examining only the combined effects of anthropogenic
160 aerosols and GHGs, which also have yet to quantify dust response to future climate
161 change due to individual changes in anthropogenic aerosols and GHGs for pursuing
162 carbon neutrality goals (Zhao et al., 2023; Liu et al., 2024). In this study, we conduct
163 Earth system model experiments to assess the impact of aerosols and GHGs reductions
164 toward carbon neutrality on meteorological variables such as precipitation, relative
165 humidity, and wind speed, as well as their implications for dust emissions and
166 concentrations. Although dust is from both natural and anthropogenic sources. This
167 study only focuses on dust from natural sources without considering anthropogenic dust.
168 Given that the combined contribution of dust sources from the North Africa and Asia
169 exceeds 80% of global dust emissions, this study strategically focuses on the dust belt
170 regions, including the Sahara Desert, Central Asia Desert, Arabian Desert, Taklamakan
171 Desert, and Gobi Desert. The findings of this study aim to provide valuable insights to
172 guide the establishment of dust prevention measures and strategies in global pursuit of
173 carbon neutrality. The paper is structured as follows. The method and data are presented
174 in Sect. 2. The results of dust changes related to the reductions in GHGs and aerosols
175 are shown in Sect. 3. The discussion and the conclusions are given in Sect. 4.

176

177 **2. Methods**

178 **2.1 Model Description**

179 The fully coupled Community Earth System Model version 1.2.2 (CESM1)
180 (Hurrell et al., 2013) is used to investigate the effects of meteorological changes
181 induced by anthropogenic aerosols and GHGs under carbon neutrality on dust
182 emissions and concentrations. The atmospheric component utilizes the Community
183 Atmosphere Model version 5 (CAM5), which simulates the major aerosol species,

184 including sulfate, black carbon, primary organic aerosol, secondary organic aerosol,
185 mineral dust and sea salt. These aerosols are distributed in the four lognormal size
186 distribution modes (i.e., Aitken, accumulation, coarse, and primary carbon modes) (Liu
187 et al., 2016). Simulations are conducted at $1.9^\circ \times 2.5^\circ$ horizontal resolution with 30
188 vertical layers. Aerosol particles within the same mode are mixed internally, whereas
189 external mixing assumption is treated for particles between different modes. The dust
190 emission flux is calculated using the Dust Entrainment and Deposition model
191 developed by Zender et al. (2003), which is implemented in the Community Land
192 Model version 4 (CLM4; Oleson et al., 2010). Dust particles are divided into four bins
193 (0.1-1.0, 1.0-2.5, 2.5-5.0, and 5.0-10.0 μm) in CLM4, and subsequently redistributed to
194 four modes of the Modal Aerosol Module scheme. The emission or mobilization
195 process is governed by the synergistic effects of multiple controlling parameters,
196 including wind friction speed, vegetation cover, and surface soil moisture content.
197 Aerosol direct and indirect radiative effects are incorporated in CAM5 (Ma et al., 2022).
198 Furthermore, optimized parameterization schemes for key aerosol processes in CAM5,
199 such as convective transport and wet deposition, have been implemented to enhance
200 model performance (Wang et al., 2013). The dynamic oceanic component in CESM1
201 uses the Parallel Ocean Program version 2 (POP2). In this study, emissions of aerosols
202 and precursors and GHGs concentrations are obtained from the CMIP6 input data,
203 specifically adopting the SSP1-1.9 and SSP5-8.5 (shared socioeconomic pathways).
204 Future emission inventories build on the Shared Socioeconomic Pathways, providing
205 standardized multidimensional parameters (e.g., population, economy, technology,
206 environment, institutions) and qualitative narratives at national/regional scales (van
207 Vuuren et al., 2017; Kriegler et al., 2017; Fujimori et al., 2017; Calvin et al., 2017;
208 Fricko et al., 2017).

209 **2.2 Experimental Design**

210 To quantify the impacts of anthropogenic aerosols and GHGs on future dust
211 toward carbon neutrality, four sets of CESM1 equilibrium simulations are designed,
212 comprising one baseline (Fut_SSP585) and three sensitivity experiments
213 (Fut_CNeutral, AA_CNeutral and GHG_CNeutral). The SSP1-1.9 represents a
214 sustainable development scenario focused on ecological restoration, conservation, and
215 a significant reduction in fossil fuel dependence. This pathway is considered the most
216 likely to achieve the 1.5°C target under the Paris Agreement and carbon neutrality in

217 the mid-21st century (Su et al., 2021; Wang et al., 2023; Zhu et al., 2024). In contrast,
218 the SSP5-8.5 follows a high fossil fuel consumption with substantial associated
219 emissions (Meinshausen et al., 2020). Many countries had committed to achieving
220 carbon neutrality by 2050 or 2060, with most targets set for the post-2050 period (Chen
221 et al., 2022). Focusing on the year 2060 therefore ensures direct alignment with policy
222 timelines and enhances the practical relevance of our results.

223 The `Fut_SSP585` simulation prescribes global GHGs concentrations and
224 anthropogenic emissions of aerosols and precursors from the CMIP6 input data, with
225 all forcings held at 2060 levels under the SSP5-8.5 scenario. In `Fut_CNeutral`
226 experiment, GHGs concentrations, aerosols, and their precursor emissions are adopted
227 following SSP1-1.9 emission pathway in 2060, enabling isolation of combined effects
228 of aerosols and GHGs through comparison with the baseline. The `AA_CNeutral`
229 experiment applies anthropogenic emissions of aerosols and precursors from SSP1-1.9
230 while retaining GHGs concentrations under SSP5-8.5, allowing aerosol effect
231 quantification by comparing with the baseline. Conversely, we also perform the
232 `GHG_CNeutral` simulations in which GHGs concentrations are set to the 2060 levels
233 under SSP1-1.9, along with aerosol emissions using SSP5-8.5 input data, which allows
234 comparison with the baseline to estimate the climate impacts of GHGs. One additional
235 experiment, `Fut_2020`, is also performed for the model evaluation, with GHGs
236 concentrations and aerosol emissions set to the 2020 levels under SSP1-1.9. All
237 simulations are initialized with the same conditions and only the GHGs concentrations
238 and/or aerosol emissions change in time and space every month. All experiments are
239 conducted with three ensemble members of different initial conditions, achieved by
240 applying a small initial perturbation to atmospheric temperature. Each ensemble
241 member is run for 100 years, with the initial 40 years considered as model spin-up
242 period, retaining the latter 60 years for analysis.

243 **2.3 Model Evaluation**

244 Numerous studies documented the hemispheric asymmetry of global dust sources,
245 with most emissions originated from northern hemisphere arid zones, notably North
246 Africa, Central Asia, East Asia, and the Middle East (Shao et al., 2011; Ginoux et al.,
247 2012; Yang et al., 2022). Consistent with prior studies that highlight peak dust activities
248 during boreal spring and summer in these regions (Ginoux et al., 2012; Nabavi et al.,
249 2016; Jethva et al., 2005, Choobari et al., 2014), our seasonal analysis for simulations

250 in 2060 also reveals substantially elevated dust emissions and concentrations in warm
251 seasons, especially spring, compared to autumn and winter (Figure 1). In this study, we
252 mainly focus on spring dust activities. To evaluate model's dust simulation performance,
253 dust optical depth from model results in boreal spring of 2020 is compared with
254 CALIPSO satellite retrievals averaged over 2017–2021. The model reasonably
255 reproduces the overall spatial distribution of dust optical depth (Figure 2), but
256 overestimates dust loading over parts of Central Asia, Eastern Africa and the Gobi
257 Desert. Similar discrepancies have been noted in existing studies, indicating that the
258 deviations between the model and observations are primarily attributable to the
259 topographic source function and the dust emission scheme used in the model (Wu et al.,
260 2020), which could potentially lead to bias in the quantitative analysis of the results.

261 **3 Results**

262 **3.1 Changing dust aerosol toward carbon neutrality**

263 Figures 3a and 3b present the spatial patterns of changes in emission fluxes and
264 near-surface concentrations of dust aerosols between carbon neutrality (SSP1-1.9) and
265 high fossil fuel (SSP5-8.5) scenarios driven by both fixed anthropogenic aerosols and
266 GHGs in 2060. Under the strong decline in anthropogenic emissions toward carbon
267 neutrality, marked reductions in dust emissions (3–12%) and concentrations (4–16%)
268 are observed across primary source regions (Figure 4a-b), particularly the North African
269 dust belt and Central Asian arid corridor, whereas increases in dust emission (3–12%)
270 and concentrations (4–8%) are found over East Asian dust source regions. Dust
271 concentrations in most regions exhibit reductions, exceeding $40 \mu\text{g m}^{-3}$ over North
272 Africa and Central Asia, while northwestern China and the North China Plain show a
273 weak increase in dust concentrations.

274 The simulated future changes in dust concentrations are the combined effects of
275 the reduction of anthropogenic aerosols and GHGs. Here we also investigate their
276 respective impacts on future dust changes through sensitivity experiments. Figures 3c-
277 d illustrate the responses of emission fluxes and near-surface concentrations of dust to
278 anthropogenic aerosol reductions in SSP1-1.9 relative to SSP5-8.5, while 3e-f
279 demonstrate the responses to GHGs reduction alone. The future reductions in
280 anthropogenic aerosols would lead to significant increases in dust emissions (6–12%)
281 and concentrations (4–20%) across the dust belt (Figure 4c-d). However, GHGs
282 reduction induces decreases in dust loads mainly over North Africa and Central Asia.

283 These contrasting patterns indicate opposite dust responses to future reductions in
284 anthropogenic aerosols and GHGs. The following sections illustrate possible
285 mechanisms derived from the analysis of key meteorological drivers and their
286 association with emission reduction strategies.

287 **3.2 Dust increases due to anthropogenic aerosols reductions**

288 Pursuing the carbon neutrality leads to substantial reductions in anthropogenic
289 emissions of aerosols and precursors. As shown in Figure 5, CMIP6 experiments show
290 decreases exceeding 8×10^{-13} kg m⁻² s⁻¹ in anthropogenic emissions of aerosols and
291 precursors, including black carbon, sulfur dioxide and precursor gases of secondary
292 organic aerosols, over polluted eastern China, South Asia, and parts of Europe and
293 North Africa in 2060 under SSP1-1.9 scenario compared to SSP5-8.5, while primary
294 organic matter emissions slightly increase by $4-8 \times 10^{-13}$ kg m⁻² s⁻¹. Although
295 anthropogenic aerosol emission changes are primarily concentrated in Asia, reductions
296 in aerosol optical depth (AOD) of approximately 0.01–0.05 are also evident over remote
297 regions including Northern Africa (Figure 6a), mainly due to the decreases in sulfate
298 aerosol (Figures 6b and 6c). Along with the aerosol reduction, the surface downwelling
299 shortwave radiation increases by 4–12W m⁻² (Figure 7a), which further increases the
300 land surface temperatures by more than 0.6 °C over eastern China, Southeast Asia and
301 North Africa and 0.9 °C over South Asia (Figure 7b). Enhanced convective instability
302 due to the warmer surface condition elevates planetary boundary layer (PBL) heights
303 over most land regions (Figure 7c). Furthermore, diminished atmospheric heating from
304 light-absorbing aerosols (e.g., black carbon) in the air reduces lower tropospheric
305 stability, intensifying convective conditions and resulting in an increase in the PBL
306 height. The associated strengthening of vertical exchange processes enhances near-
307 surface wind speeds by 0.05–0.1 m s⁻¹ through downward momentum transfer (Figure
308 8a) (Qin et al., 2024). Note that, the spatial patterns of changes in PBL height show a
309 mismatch with dust emission changes in some regions, which arises from the imperfect
310 correspondence between boundary layer height and surface wind speed and has been
311 reported in many studies (e.g., Jacobson et al. 2006; Qin et al., 2024). The wind speed
312 responses to aerosol changes reported in these studies agrees with our findings, and the
313 mechanistic interpretation that aerosol reduction increases wind speed is also consistent
314 with their established physical understanding. Related to the surface warming driven
315 by anthropogenic aerosol reductions, relative humidity and soil water content decrease

316 (Figures 8b-c). These changes in meteorological and land surface conditions explain
317 the simulated increases (exceeding $2 \times 10^{-9} \text{ kg m}^{-2} \text{ s}^{-1}$) in dust emissions across the dust
318 belt due to the anthropogenic aerosol reductions toward carbon neutrality (Figure 3c).
319 This result is consistent with previous studies (Menut et al., 2019; Xie et al., 2025).

320 Previous studies have established a robust positive correlation between near-
321 surface wind speed and dust emission fluxes, particularly in arid dust source regions
322 characterized by chronically low soil moisture and minimal precipitation inputs (Zender
323 et al., 2003; Dong et al., 2006). Our analysis reveals that anthropogenic aerosol
324 reductions in SSP1-1.9 relative to SSP5-8.5 amplify 10-m wind speed by 0.05–0.10 m
325 s^{-1} across core dust sources (Figures 8a), driving intensified dust emission fluxes (6–
326 12%) and near-surface concentrations (8–16%) in North and Central Africa (Figures
327 3c-d, Figures 4c-d). The dust-wind speed relationship is modulated by emission
328 thresholds. In arid areas, the threshold of wind speed for dust mobilization increases
329 with rising relative humidity (Ravi et al., 2005). This is primarily due to the enhanced
330 adsorption layer interactions created by overlapping water films on adjacent soil
331 particles (Ravi et al., 2005). Consequently, after the reduction of anthropogenic aerosols,
332 reduced relative humidity by –1% to –3% (Figure 8b) lowers the critical threshold of
333 wind speed, particularly in Central Africa and East Asia. Additionally, in the major dust
334 source regions, precipitation changes are minimal and statistically insignificant (Figure
335 8d), which do not have a large influence on dust concentrations after emitting into the
336 atmosphere.

337 **3.3 Dust decreases due to greenhouse gas reductions**

338 Figure 9a illustrates the surface temperature distribution in 2060 under SSP5-8.5,
339 highlighting persistent land-ocean thermal contrast with continental temperatures
340 around dust source regions much higher than oceanic values. Due to GHGs reductions
341 in SSP1-1.9 relative to SSP5-8.5, surface temperatures decrease by 1.8–3.0 °C over
342 land and 1.2–1.8 °C over adjacent oceans (Figure 9b), where the overall land-sea
343 contrast is largely due to the higher heat capacity of water than land surface. Figures 9c
344 and 9d respectively depict the zonal and meridional distributions of surface
345 temperatures over the Sahara Desert of North Africa. Notably, the surface cooling due
346 to GHGs reductions is stronger over the Sahara Desert (10°–30°N, 10°W–30°E) than
347 that over the Mediterranean Sea (north of 30°N) and North Atlantic Ocean (west of
348 10°W). It diminishes the land-sea temperature gradient, thereby contributing to the

349 decline in wind speed over North Africa (Figure 10a). Central Asia Desert also
350 demonstrates a stronger temperature reduction than the surrounding Caspian Sea
351 (Figure 9e) and high latitude regions, weakening the land-sea thermal gradient and
352 thereby driving the decrease in surface wind speed throughout Central Asia (Figure
353 10a). By reducing the land-ocean thermal contrast, GHG mitigation lowers surface
354 wind speeds over major dust source regions, leading to a consequent decline in dust
355 emissions (exceeding $2 \times 10^{-9} \text{ kg m}^{-2} \text{ s}^{-1}$) (Figure 3e), which is consistent with previous
356 study. Qu et al. (2025) studied prolonged wind droughts in a warming climate. Under
357 the SSP5-8.5 scenario, they found that wind droughts decreased in the tropics, primarily
358 due to increased wind speeds. Reversely, in the tropics, global warming amplifies the
359 land-ocean thermal contrast, thereby strengthening winds. Thus, the mechanism of
360 wind speed reduction is consistent with established understanding. As a result of the
361 GHGs reduction implementation, the marked temperature reduction suppresses surface
362 evaporation and alters atmospheric saturation vapor pressure, thereby increasing
363 relative humidity by 1–3% across Northern Hemisphere dust source areas (Figure 10b).

364 Dust emission suppression in North African and Central Asian regions (Figure 3e)
365 is primarily attributed to the weakened surface wind speeds induced by GHGs reduction
366 (Figure 10a). The GHGs reduction elevates relative humidity (Figure 10b), which raises
367 the critical threshold wind velocity required for dust mobilization. It further reduces
368 dust emission fluxes by 6–15% and atmospheric dust concentrations by 8–20% (Figure
369 4e-f), particularly in the North African and Central Asian source regions, even though
370 the soil moisture slightly increases in some regions (Figure 10c). This finding is
371 consistent with previous research indicating that dust emissions across most source
372 regions are significantly lower under the low-emission scenarios than under high-
373 emission scenarios (Zhao et al., 2023; Liu et al., 2024; Gomez et al., 2023). The
374 precipitation does not show significant changes over the North Africa and Central Asia
375 (Figure 10d). Over East Asia, the decreases in precipitation and soil water, likely related
376 to the changing atmospheric circulation and moisture transport due to GHGs reductions,
377 slightly promote the dust emissions over some parts of Taklamakan Desert and Gobi
378 Desert (Figure 3e). However, decreases in wind speed do not favor the dust transport
379 (Figure 10a) and are conducive to the local dust deposition. It can be confirmed by the
380 changes in dust deposition that more dust is removed from the atmosphere over the
381 Taklamakan Desert and the downwind North China Plain (Figure 11) and the increase
382 in dust removal surpasses the increase in dust emission (0.5×10^{-9} to $2 \times 10^{-9} \text{ kg m}^{-2} \text{ s}^{-1}$)

383 (Figure 3e).

384 **4 Discussions and Conclusions**

385 In the carbon-neutral future scenario, reductions in GHGs and aerosols for climate
386 mitigation and environmental improvement could change meteorological conditions
387 and further influence dust emissions and concentrations. However, critical knowledge
388 gaps remain in dust response to future climate change for pursuing carbon neutrality
389 goals. While existing work has captured the combined impacts of anthropogenic
390 aerosols and GHGs on dust flux under different future scenarios (Singh et al., 2017;
391 Woodward et al., 2005; Zhao et al., 2023; Liu et al., 2024), the distinct roles of
392 anthropogenic aerosols versus GHGs in modulating dust flux remain unresolved. Our
393 work systematically resolves these knowledge gaps. In this study, the individual
394 impacts of anthropogenic aerosols and GHGs reductions under the global carbon
395 neutral scenario on dust emissions and concentrations over the dust belt of low- to mid-
396 latitudes in the Northern Hemisphere are investigated using the fully coupled CESM1
397 model. The distinct effects of future GHGs and aerosol emission changes on dust
398 emissions are individually assessed. Under carbon neutral scenario (SSP1-1.9),
399 significant reductions in dust emissions (3–12%) and concentrations (4–16%) are seen
400 over major Asian and African dust source regions relative to the high fossil fuel scenario
401 (SSP5-8.5) in 2060 (Figures 4a-b).

402 Anthropogenic aerosols and GHGs reduction exert opposite impacts on dust
403 emissions. Due to aerosol reductions toward carbon neutrality, atmospheric convective
404 is amplified, elevating surface wind speeds by $0.05\text{--}0.10\text{ m s}^{-1}$ and intensifying dust
405 emissions (exceeding $2\times10^{-9}\text{ kg m}^{-2}\text{ s}^{-1}$) and concentrations (exceeding $30\text{ }\mu\text{g m}^{-3}$),
406 particularly in the North African, Central Asian, South Asian, and East Asian source
407 sectors, by year 2060. Additionally, the reduction in aerosols is expected to increase
408 near-surface temperature by $0.3\text{--}1.2^\circ\text{C}$, decreasing relative humidity and soil water
409 content, further intensifying dust emissions. In contrast, GHGs reduction diminishes
410 the land-ocean thermal contrast, suppressing surface winds by $0.01\text{--}0.1\text{ m s}^{-1}$ and
411 associated dust emissions by $2\times10^{-9}\text{ kg m}^{-2}\text{ s}^{-1}$ and concentrations by $50\text{ }\mu\text{g m}^{-3}$ in North
412 Africa and Central Asia (Figures 3e-f). The marked temperature reduction also elevates
413 relative humidity by 1–3%, suppressing dust generation, due to the GHGs reductions.
414 Dust emissions over parts of the Taklamakan Desert and Gobi Desert are promoted,
415 because of a decrease in precipitation and soil water. However, decreases in wind speed

416 enhance dust deposition, leading to a decline in near-surface dust concentrations.

417 Under combined GHG and aerosol reductions, dust emissions decline by 3%–12%
418 across Northern Africa and Central Asia, contrasting with an increase of 3%–9% in East
419 Asia (Figures 4a-b). [A consistent pattern has been observed in previous research \(Liu
420 et al., 2024\)](#). Correspondingly, surface wind speeds decrease by 0.01–0.1 m/s across
421 Northern Africa and Central Asia but increase by 0.01–0.05 m/s over East Asia (Figure
422 12a). Concurrently, relative humidity rises more significantly by 0.1%–3% over major
423 dust source regions (Figure 12b). This increase raises the wind speed threshold for dust
424 emission, thereby suppressing dust uplift. However, in East Asia, higher wind speeds
425 offset the suppression from increased humidity. Changes in soil moisture and
426 precipitation are insignificant in these dust source regions and thus play minor roles in
427 dust emission (Figure 12c-d). Consequently, the suppressive effect of GHG mitigation
428 dominates over the promotive effect of aerosol mitigation in Northern Africa and
429 Central Asia. This outcome primarily results from the stronger cooling effect induced
430 by GHG reductions compared to the warming caused by anthropogenic aerosol
431 reductions (Figure 13a). The cooling diminishes the land–ocean thermal contrast across
432 Africa and Central Asia, further suppressing wind speeds and inhibiting dust emissions
433 (Figure 13b-d). In contrast, elevated wind speeds over East Asia are linked to an
434 intensified Mongolia–Siberian High under joint mitigation, as indicated by sea level
435 pressure increases of 40–80 Pa in Figure 13e. This enhanced pressure gradient
436 strengthens surface winds and promotes dust emissions across source regions in East
437 Asia. This study addresses the critical knowledge gaps about the dust response to future
438 climate change for pursuing carbon neutrality, providing valuable insights to guide the
439 establishment of dust prevention measures and strategies in global pursuit of carbon
440 neutrality.

441 It is noteworthy that the responses of dust emissions and concentrations to the
442 GHG and aerosol mitigation are not linear. Adding the individual effects of GHGs and
443 aerosols together, dust emissions and concentrations show less decreases and even
444 increases in over the Northern Hemisphere dust belt (Figure S1), compared to the
445 combined effect of GHG and aerosol mitigation (Figure 3). The differences are likely
446 associated with nonlinear response of wind fields, including both the wind direction
447 and wind speed, to the temperature changes induced by GHGs and aerosols, which
448 could offset each other and ultimately lead to divergent responses in dust emissions and
449 concentrations.

450 Dust emissions in the Northern Hemisphere reach a maximum in spring, the
451 predominant season for dust storm occurrence. Therefore, this study focuses primarily
452 on dust variations in the spring. Nevertheless, changes in the annual mean dust
453 emissions are also important. Annual mean dust emission changes are highly consistent
454 with spring patterns, showing increased emissions from aerosol reductions and
455 decreased emissions from GHGs mitigation (Figure S2).

456 Although large model uncertainties exist in the projections of climate response to
457 anthropogenic forcings, and climate simulated in CESM is relatively more sensitive to
458 anthropogenic forcings than many other global models (Wang et al., 2023; Ren et al.,
459 2024), inter-model comparisons nevertheless yield consistent results regarding dust
460 emissions under the SSP1-1.9 and SSP5-8.5 scenarios. Specifically, many CMIP6
461 models indicate that GHG and aerosol mitigation reduces dust emissions in Northwest
462 Africa (Figure S3), similar to the CESM simulation. Under future scenario, potential
463 variations in tropospheric ozone concentrations may introduce additional complexity,
464 as ozone can modulate key meteorological drivers as a greenhouse gas (Wang et al,
465 2023; Gao et al, 2022), which can also regulate dust emission processes. It is reasonable
466 to speculate that the decline in ozone concentrations under carbon neutrality pathways
467 would lead to a greater reduction in dust emissions relative to SSP5-8.5 than is currently
468 estimated in this study, if this factor were accounted for. Also, this study does not
469 consider the land cover change and the potential future forest expansion (Cramer et al.,
470 2001; Notaro et al., 2007; Jiang et al., 2011) may weaken the dust changes toward
471 carbon neutrality, which deserves further investigation in future work. Furthermore, as
472 evidenced in our model validation, the CESM dust simulations exhibit inherent
473 limitations, primarily originating from the topographic source function, the dust
474 emission scheme, coarse spatial and vertical model resolution, and PBL
475 parameterization (Wu et al., 2020; Lindvall et al., 2012), which collectively contribute
476 to systematic biases in dust emission flux estimates.

477 Our findings demonstrate that the carbon neutrality scenario leads to an overall
478 reduction in dust emissions compared to the high fossil fuel scenario, thereby
479 alleviating future pressures on dust control policies. These results highlight the
480 importance of advancing carbon neutrality, which not only achieves climate mitigation
481 targets but also helps reduce dust pollution. Notably, however, East Asia exhibits
482 anomalous increases in dust emissions. Therefore, while implementing carbon
483 neutrality policies, it is essential to additionally strengthen regional measures such as

484 afforestation and the construction of protective forest belts to further prevent dust
485 storms.

486 **Author contributions.** YY designed the research; SY performed the simulations and
487 analyzed the data. All authors including LR, HW, PW, LC, JJ and HL discussed the
488 results and wrote the paper.

489

490 **Acknowledgments.** The Pacific Northwest National Laboratory is operated for the U.S.
491 Department of Energy by the Battelle Memorial Institute under contract DE-AC05-
492 76RLO1830.

493

494 **Financial support.** This study was supported by the National Key Research and
495 Development Program of China (Grant 2024YFF0811400), National Natural Science
496 Foundation of China (Grant 42475032), Natural Science Foundation of the Jiangsu
497 Higher Education Institutions of China (Grant 24KJB170007), and Jiangsu Innovation
498 and Entrepreneurship Team (Grant JSSCTD202346).

499

500 **Conflict of Interest.** At least one of the (co-)authors is a member of the editorial board
501 of ACP.

502

503 **Code and data availability.** The dust optical depth for 2020 level can be obtained from
504 CALIPSO satellite retrievals
505 (https://search.earthdata.nasa.gov/search/granules?p=C1633034978-LARC_ASDC,
506 last access: 1 June 2025). The CESM model is publicly available at
507 <http://www.cesm.ucar.edu/models/> (last access: 1 June 2025). The processed modeling
508 data are available at <https://doi.org/10.5281/zenodo.15478736> (last access: 1 June 2025).

509 **References**

- 510 Akinsanola, A. A., Adebiyi, A. A., Bobde, V., Adeyeri, O. E., Tamoffo, A. T., and Danso,
511 D. K.: Projected changes in African easterly wave activity due to climate change,
512 *Commun. Earth Environ.*, 6, 2, <https://doi.org/10.1038/s43247-024-01981-9>, 2025.
- 513 Banerjee, P., Satheesh, S. K., and Krishna Moorthy, K.: Is the Atlantic Ocean driving
514 the recent variability in South Asian dust?, *Atmos. Chem. Phys.*, 21, 17665–17685,
515 <https://doi.org/10.5194/acp-21-17665-2021>, 2021.
- 516 Calvin, K., Bond-Lamberty, B., Clarke, L., Edmonds, J., Eom, J., Hartin, C., Kim, S.,
517 Kyle, P., Link, R., Moss, R., McJeon, H., Patel, P., Smith, S., Waldhoff, S., and
518 Wise, M.: The SSP4: A world of deepening inequality, *Global Environ. Change*,
519 42, 284–296, 2017.
- 520 Chen, L., Msigwa, G., Yang, M., Osman, A. I., Fawzy, S., Rooney, D. W., and Yap, P-
521 S.: Strategies to achieve a carbon neutral society: a review, *Environ. Chem. Lett.*,
522 20, 2277–2310, <https://doi.org/10.1007/s10311-022-01435-8>, 2022.
- 523 Chen, Y., Chen, S., Bi, H., Zhou, J., and Zhang, Y.: Where is the Dust Source of 2023
524 Several Severe Dust Events in China?, *Bull. Amer. Meteor. Soc.*, 105, E2085–
525 E2096, <https://doi.org/10.1175/BAMS-D-23-0121.1>, 2024.
- 526 Chen, Z., Zhou, T., Zhang, W., Li, P., and Zhao, S.: Projected changes in the annual
527 range of precipitation under stabilized 1.5°C and 2.0°C warming futures, *Earth's
528 Future*, 8, e2019EF001435, <https://doi.org/10.1029/2019EF001435>, 2020.
- 529 Choobari, O. A., Zawar-Reza, P., and Sturman, A.: The global distribution of mineral
530 dust and its impacts on the climate system: A review, *Atmos. Res.*, 138, 152-165,
531 <https://doi.org/10.1016/j.atmosres.2013.11.007>, 2014.
- 532 Cramer, W., Bondeau, A., Woodward, F. I., Prentice, I. C., Betts, R. A., Brovkin, V.,
533 Cox, P. M., Fisher, V., Foley, J. A., Friend, A. D., Kucharik, C., Lomas, M. R.,
534 Ramankutty, N., Sitch, S., Smith, B., White, A., and Young-Molling, C.: Global
535 response of terrestrial ecosystem structure and function to CO₂ and climate change:
536 Results from six dynamic global vegetation models, *Global. Change Biology*, 7(4),
537 357-373, <https://doi.org/10.1046/j.1365-2486.2001.00383.x>, 2001.
- 538 Das, S., Giorgi, F., Giuliani, G., Dey, S., and Coppola, E.: Near-future anthropogenic
539 aerosol emission scenarios and their direct radiative effects on the present-day
540 characteristics of the Indian summer monsoon, *J. Geophys. Res-atmos.*, 125,
541 e2019JD031414, <https://doi.org/10.1029/2019JD031414>, 2020.
- 542 Dong, Z., Wang, H., Qian, G., Luo, W., and Zhang, Z.: Wind shear with a blowing-sand
543 boundary layer, *Geophys. Res. Lett.*, 33, L22804,
544 <https://doi.org/10.1029/2006GL026739>, 2006.
- 545 Francis, D., Fonseca, R., Nelli, N., Teixido, O., Mohamed, R., and Perry, R.: Increased
546 Shamal winds and dust activity over the Arabian Peninsula during the COVID-19
547 lockdown period in 2020, *Aeolian Res.*, 55, 100786,
548 <https://doi.org/10.1016/j.aeolia.2022.100786>, 2022.

- 549 Fricko, O., Havlik, P., Rogelj, J., Klimont, Z., Gusti, M., Johnson, N., Kolp, P.,
550 Strubegger, M., Valin, H., Amann, M., Ermolieva, T., Forsell, N., Herrero, M.,
551 Heyes, C., Kindermann, G., Krey, V., McCollum, D. L., Obersteiner, M., Pachauri,
552 S., Rao, S., Schmid, E., Schoepp, W., and Riahi, K.: The marker quantification of
553 the Shared Socioeconomic Pathway 2: A middle-of-the-road scenario for the 21st
554 century, *Global Environ. Change*, 42, 251–267,
555 <https://doi.org/10.1016/j.gloenvcha.2016.06.004>, 2017.
- 556 Fujimori, S., Hasegawa, T., Masui, T., Takahashi, K., Herran, D. S., Dai, H., Hijioka,
557 Y., and Kainuma, M.: SSP3: AIM implementation of shared socioeconomic
558 pathways, *Global Environ. Change*, 42, 268–283,
559 <https://doi.org/10.1016/j.gloenvcha.2016.06.009>, 2017.
- 560 Fussell, J. C., and Kelly, F. J.: Mechanisms underlying the health effects of desert sand
561 dust, *Environ. Int.*, 157, 106790, <https://doi.org/10.1016/j.envint.2021.106790>,
562 2021.
- 563 Gao, J., Yang, Y., Wang, H., Wang, P., Li, H., Li, M., Ren, L., Yue, X., and Liao, H.:
564 Fast climate responses to emission reductions in aerosol and ozone precursors in
565 China during 2013–2017, *Atmos. Chem. Phys.*, 22, 7131–7142,
566 <https://doi.org/10.5194/acp-22-7131-2022>, 2022.
- 567 Ginoux, P., Prospero, J. M., Gill, T. E., Hsu, N. C., and Zhao, M.: Global-scale
568 attribution of anthropogenic and natural dust sources and their emission rates
569 based on MODIS Deep Blue aerosol products, *Rev. Geophys.*, 50, RG3005,
570 <https://doi.org/10.1029/2012RG000388>, 2012.
- 571 Ginoux, P., Prospero, J. M., Torres, O., and Chin, M.: Long-term simulation of global
572 dust distribution with the GOCART model: correlation with North Atlantic
573 Oscillation, *Environ. Modell. Softw.*, 19, 113-128, [https://doi.org/10.1016/S1364-8152\(03\)00114-2](https://doi.org/10.1016/S1364-8152(03)00114-2), 2004.
- 575 Gomez, J., Allen, R. J., Turnock, S. T., Horowitz, L. W., Tsagiris, K., Bauer, S. E.,
576 Olivié, D., Thomson, E. S., and Ginoux, P.: The projected future degradation in air
577 quality is caused by more abundant natural aerosols in a warmer world, *Commun.
578 Earth Environ.*, 4, 22, <https://doi.org/10.1038/s43247-023-00688-7>, 2023.
- 579 Goudie, A. S.: Desert dust and human health disorders, *Environ. Int.*, 63, 101-113,
580 <https://doi.org/10.1016/j.envint.2013.10.011>, 2014.
- 581 Griffin, D. W.: Atmospheric Movement of Microorganisms in Clouds of Desert Dust
582 and Implications for Human Health, *Clin. Microbiol. Rev.*, 20, 459-477,
583 <https://doi.org/10.1128/cmr.00039-06>, 2007.
- 584 Gui, K., Yao, W., Che, H., An, L., Zheng, Y., Li, L., Zhao, H., Zhang, L., Zhong, J.,
585 Wang, Y., and Zhang, X.: Record-breaking dust loading during two mega dust
586 storm events over northern China in March 2021: aerosol optical and radiative
587 properties and meteorological drivers, *Atmos. Chem. Phys.*, 22, 7905–7932,
588 <https://doi.org/10.5194/acp-22-7905-2022>, 2022.

- 589 Hu, Z., Ma, Y., Jin, Q., Idrissa, N. F., Huang, J., and Dong, W.: Attribution of the March
590 2021 exceptional dust storm in North China, *Bull. Am. Meteorol. Soc.*, 104, E749–
591 E755, <https://doi.org/10.1175/BAMS-D-22-0151.1>, 2023.
- 592 Hurrell, J. W., Holland, M. M., Gent, P. R., Ghan, S., Kay, J. E., Kushner, P. J.,
593 Lamarque, J. F., Large, W. G., Lawrence, D., Lindsay, K., Lipscomb, W. H., Long,
594 M. C., Mahowald, N., Marsh, D. R., Neale, R. B., Rasch, P., Vavrus, S., Vertenstein,
595 M., Bader, D., Collins, W. D., Hack, J. J., Kiehl, J., and Marshall, S.: The
596 Community Earth System Model: A Framework for Collaborative Research, *Bull.*
597 *Am. Meteor. Soc.*, 94, 1339–1360, <https://doi.org/10.1175/BAMS-D-12-00121.1>,
598 2013.
- 599 Jacobson, M. Z., and Kaufman, Y. J.: Wind reduction by aerosol particles, *Geophys.*
600 *Res. Lett.*, 33, L24814, <https://doi.org/10.1029/2006GL027838>, 2006.
- 601 Jethva, H., Satheesh, S. K., and Srinivasan, J.: Seasonal variability of aerosols over the
602 Indo-Gangetic basin, *J. Geophys. Res.*, 110, D21204,
603 <https://doi.org/10.1029/2005JD005938>, 2005.
- 604 Jiang, D., Zhang, Y. and Lang, X.: Vegetation feedback under future global warming,
605 *Theor. Appl. Climatol.*, 106, 211–227, <https://doi.org/10.1007/s00704-011-0428-6>, 2011.
- 606 Jickells, T. D., An, Z. S., Andersen, K. K., Baker, A. R., Bergametti, G., Brooks, N.,
607 Cao, J. J., Boyd, P. W., Duce, R. A., Hunter, K. A., Kawahata, H., Kubilay, N.,
608 Laroche, J., Liss, P. S., Mahowald, N., Prospero, J. M., Ridgwell, A. J., Tegen, I.,
609 and Torres, R.: Global Iron Connections Between Desert Dust, Ocean
610 Biogeochemistry, and Climate, *Science*, 308, 67-71,
611 <https://doi.org/10.1126/science.1105959>, 2005.
- 612 Kok, J. F., Adebiyi, A. A., Albani, S., Balkanski, Y., Checa-Garcia, R., Chin, M.,
613 Colarco, P. R., Hamilton, D. S., Huang, Y., Ito, A., Klose, M., Li, L., Mahowald,
614 N. M., Miller, R. L., Obiso, V., Pérez García-Pando, C., Rocha-Lima, A., and Wan,
615 J. S.: Contribution of the world's main dust source regions to the global cycle of
616 desert dust, *Atmos. Chem. Phys.*, 21, 8169–8193, <https://doi.org/10.5194/acp-21-8169-2021>, 2021.
- 617 Kok, J. F., Ridley, D. A., Zhou, Q., Miller, R. L., Zhao, C., Heald, C. L., Ward, D. S.,
618 Albani, S., and Haustein, K.: Smaller desert dust cooling effect estimated from
619 analysis of dust size and abundance, *Nat. Geosci.*, 10, 274–278,
620 <https://doi.org/10.1038/ngeo2912>, 2017.
- 621 Kok, J. F., Storelvmo, T., Karydis, V.A., Adebiyi, A. A., Mahowald, N. M., Evan, A. T.,
622 He, C., and Leung, D. M.: Mineral dust aerosol impacts on global climate and
623 climate change, *Nat. Rev. Earth Environ.*, 4, 71–86,
624 <https://doi.org/10.1038/s43017-022-00379-5>, 2023.
- 625 Kriegler, E., Bauer, N., Popp, A., Humpenöder, F., Leimbach, M., Strefler, J.,
626 Baumstark, L., Bodirsky, B. L., Hilaire, J., Klein, D., Mouratiadou, I., Weindl, I.,

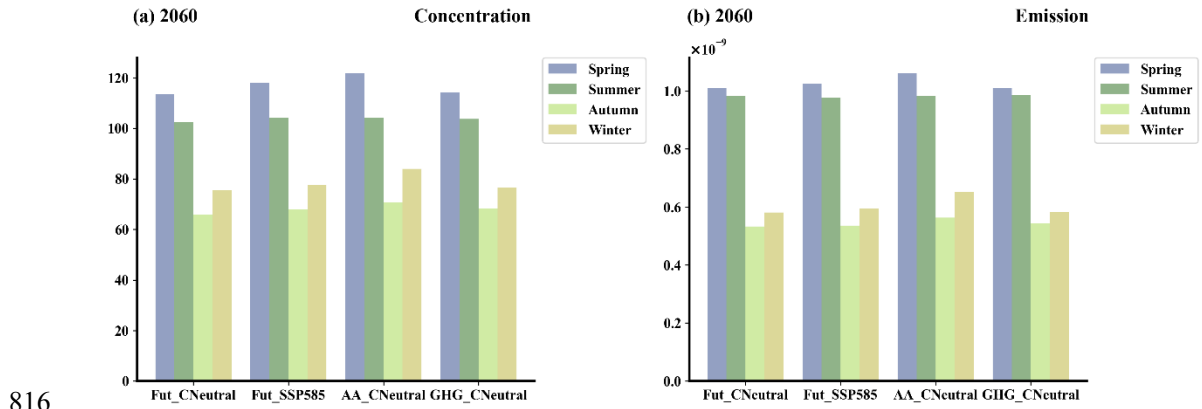
- 629 Bertram, C., Dietrich, J.-P., Luderer, G., Pehl, M., Pietzcker, R., Piontek, F., Lotze-
630 Campen, H., Biewald, A., Bonsch, M., Giannousakis, A., Kreidenweis, U., Müller,
631 C., Rolinski, S., Schultes, A., Schwanitz, J., Stevanovic, M., Calvin, K.,
632 Emmerling, J., Fujimori, S., and Edenhofer, O.: Fossil-fueled development (SSP5):
633 an energy and resource intensive scenario for the 21st century, *Global Environ.*
634 *Change*, 42, 297–315, 2017.
- 635 Kuzmina, S. I., Bengtsson, L., Johannessen, O. M., Drange, H., Bobylev, L. P., and
636 Miles, M. W.: The North Atlantic Oscillation and greenhouse-gas forcing,
637 *Geophys. Res. Lett.*, 32, L04703, <https://doi.org/10.1029/2004GL021064>, 2005.
- 638 Lee, S., and Feldstein, S. B.: Detecting Ozone- and Greenhouse Gas–Driven Wind
639 Trends with Observational Data, *Science*, 339, 563–567,
640 <https://doi.org/10.1126/science.1225154>, 2013.
- 641 Lei, Y., Wang, Z., Wang, D., Zhang, X., Chen, H., Yue, X., Tian, C., Zhong, J., Guo, L.,
642 Li, L., Zhou, H., Liu, L., and Xu, Y.: Co-benefits of carbon neutrality in enhancing
643 and stabilizing solar and wind energy, *Nat. Clim. Chang*, 13, 693–700,
644 <https://doi.org/10.1038/s41558-023-01692-7>, 2023.
- 645 Li, B., Liao, H., Li, K., Wang, Y., Zhang, L., Guo, Y., Liu, L., Li, J., Jin, J., Yang, Y.,
646 Gong, C., Wang, T., Shen, W., Wang, P., Dang, R., Liao, K., Zhu, Q., and Jacob,
647 D. J.: Unlocking nitrogen management potential via large-scale farming for air
648 quality and substantial Co-benefits, *Natl. Sci. Rev.*, 11, nwae324,
649 <https://doi.org/10.1093/nsr/nwae324>, 2024.
- 650 Lindvall, J., Svensson, G., and Hannay, C.: Evaluation of Near-Surface Parameters in
651 the Two Versions of the Atmospheric Model in CESM1 using Flux Station
652 Observations, *J. Climate*, 26, 26–44, <https://doi.org/10.1175/JCLI-D-12-00020.1>,
653 2013.
- 654 Liu, J., Wang, X., Wu, D., Wei, H., Li, Y., and Ji, M.: Historical footprints and future
655 projections of global dust burden from bias-corrected CMIP6 models, *npj Clim.*
656 *Atmos. Sci.*, 7, 1, <https://doi.org/10.1038/s41612-023-00550-9>, 2024.
- 657 Liu, X., Chen, S., Guo, Z., Zhou, H., Chen, Y., Kang, Y., Liu, Q., Huang, G., Liu, T.,
658 Chen, C., and He, Q.: The influence of dusts on radiation and temperature over the
659 eastern Asia with a regional climate model, *Sci. Total Environ.*, 792, 148351,
660 <https://doi.org/10.1016/j.scitotenv.2021.148351>, 2021.
- 661 Liu, X., Ma, P.-L., Wang, H., Tilmes, S., Singh, B., Easter, R. C., Ghan, S. J., and Rasch,
662 P. J.: Description and evaluation of a new four-mode version of the Modal Aerosol
663 Module (MAM4) within version 5.3 of the Community Atmosphere Model,
664 *Geosci. Model Dev.*, 9, 505–522, <https://doi.org/10.5194/gmd-9-505-2016>, 2016.
- 665 Ma, X., Huang, G., and Cao, J.: The significant roles of anthropogenic aerosols on
666 surface temperature under carbon neutrality, *Sci. Bull.*, 67, 470–473,
667 <https://doi.org/10.1016/j.scib.2021.10.022>, 2022.

- 668 Meinshausen, M., Nicholls, Z. R. J., Lewis, J., Gidden, M. J., Vogel, E., Freund, M.,
669 Beyerle, U., Gessner, C., Nauels, A., Bauer, N., Canadell, J. G., Daniel, J. S., John,
670 A., Krummel, P. B., Luderer, G., Meinshausen, N., Montzka, S. A., Rayner, P. J.,
671 Reimann, S., Smith, S. J., van den Berg, M., Velders, G. J. M., Vollmer, M. K., and
672 Wang, R. H. J.: The shared socio-economic pathway (SSP) greenhouse gas
673 concentrations and their extensions to 2500, *Geosci. Model Dev.*, 13, 3571–3605,
674 <https://doi.org/10.5194/gmd-13-3571-2020>, 2020.
- 675 Meng, Q., Yan, C., Li, R., Zhang, T., Zheng, M., Liu, Y., Zhang, M., Wang, G., Du, Y.,
676 Shang, C., and Fu, P.: Variations of PM2.5-bound elements and their associated
677 effects during long-distance transport of dust storms: Insights from multi-sites
678 observations, *Sci. Total Environ.*, 889, 164062,
679 <https://doi.org/10.1016/j.scitotenv.2023.164062>, 2023.
- 680 Menut, L., Tuccella, P., Flamant, C., Deroubaix, A., and Gaetani, M.: The role of
681 aerosol-radiation-cloud interactions in linking anthropogenic pollution over
682 southern west Africa and dust emission over the Sahara, *Atmos. Chem. Phys.*, 19,
683 14657–14676, <https://doi.org/10.5194/acp-19-14657-2019>, 2019.
- 684 Min, Q. L., Li, R., Lin, B., Joseph, E., Wang, S., Hu, Y., Morris, V., and Chang, F.:
685 Evidence of mineral dust altering cloud microphysics and precipitation, *Atmos.*
686 *Chem. Phys.*, 9, 3223–3231, <https://doi.org/10.5194/acp-9-3223-2009>, 2009.
- 687 Myhre, G., Forster, P. M., Samset, B. H., Hodnebrog, Ø., Sillmann, J., Aalbergsjø, S.
688 G., Andrews, T., Boucher, O., Faluvegi, G., Fläschner, D., Iversen, T., Kasoar, M.,
689 Kharin, V., Lamarque, J. F., Olivié, D., Richardson, T., Shindell, D., Shine, K. P.,
690 Stjern, C. W., Takemura, T., Voulgarakis, A., and Zwiers, F.: PDRMIP: A
691 Precipitation Driver and Response Model Intercomparison Project, Protocol and
692 preliminary results, *Bull. Am. Meteorol. Soc.*, 98(6), 1185–1198,
693 <https://doi.org/10.1175/bams-d-16-0019.1>, 2017.
- 694 Nabavi, S. O., Haimberger, L., and Samimi, Cyrus.: Climatology of dust distribution
695 over West Asia from homogenized remote sensing data, *Aeolian Res.*, 21, 93–107,
696 <https://doi.org/10.1016/j.aeolia.2016.04.002>, 2016.
- 697 Notaro, M., Vavrus, S., and Liu, Z.: Global Vegetation and Climate Change due to
698 Future Increases in CO₂ as Projected by a Fully Coupled Model with Dynamic
699 Vegetation, *J. Climate*, 20, 70–90, <https://doi.org/10.1175/JCLI3989.1>, 2007.
- 700 Oleson, K. W., Lawrence, D. M., Bonan, G. B., Flanner, M. G., Kluzek, E., Lawrence,
701 P. J., Levis, S., Swenson, S. C., Thornton, P. E., Dai, A., and Decker, M.: Technical
702 description of version 4.0 of the Community Land Model (CLM) (NCAR/TN-
703 478+STR), University Corporation for Atmospheric Research,
704 <https://doi.org/10.5065/D6FB50WZ>, 2010.
- 705 Pabortsava, K., Lampitt, R. S., Benson, J., Crowe, C., McLachlan, R., Moigne, F. A.,
706 Moore, C. M., Pebody, C., Provost, P., Rees, A. P., Tilstone, G. H., and Woodward,

- 707 E. M. S.: Carbon sequestration in the deep Atlantic enhanced by Saharan dust, *Nat.*
708 *Geosci.*, 10, 189–194, <https://doi.org/10.1038/ngeo2899>, 2017.
- 709 Prospero, J. M., Ginoux, P., Torres, O., Nicholson, S. E., and Gill, T. E.: Environmental
710 characterization of global sources of atmospheric soil dust identified with the
711 nimbus 7 total ozone mapping spectrometer (TOMS) absorbing aerosol product,
712 *Rev. Geophys.*, 40(1), 1002, <https://doi.org/10.1029/2000RG000095>, 2002.
- 713 Qin, Y., Zhou, M., Hao, Y., Huang, X., Tong, D., Huang, L., Zhang, C., Cheng, J., Gu,
714 W., Wang, L., He, X., Zhou, D., Chen, Q., Ding, A., and Zhu, T.: Amplified
715 positive effects on air quality, health, and renewable energy under China's carbon
716 neutral target, *Nat. Geosci.*, 17, 411–418, <https://doi.org/10.1038/s41561-024-01425-1>, 2024.
- 717 Qu, M., Shen, L., Zeng, Z., Yang, B., Zhong, H., Yang, X. and Liu, X.: Prolonged wind
718 droughts in a warming climate threaten global wind power security, *Nat. Clim.
719 Chang.* 15, 842–849, <https://doi.org/10.1038/s41558-025-02387-x>, 2025.
- 720 Ramanathan, V., Crutzen, P. J., Kiehl, J. T., and Rosenfeld, D.: Aerosols, Climate, and
721 the Hydrological Cycle, *Science*, 294, 2119-2124,
722 <https://doi.org/10.1126/science.1064034>, 2001.
- 723 Ravi, S., and D'Odorico, P.: A field-scale analysis of the dependence of wind erosion
724 threshold velocity on air humidity, *Geophys. Res. Lett.*, 32, L21404,
725 <https://doi.org/10.1029/2005GL023675>, 2005.
- 726 Ren, L., Yang, Y., Wang, H., Wang, P., Yue, X., and Liao, H.: Co-benefits of mitigating
727 aerosol pollution to future solar and wind energy in China toward carbon neutrality,
728 *Geophys. Res. Lett.*, 51, e2024GL109296,
729 <https://doi.org/10.1029/2024GL109296>, 2024.
- 730 Roy, D., Kim, J., Lee, M., and Park, J.: Adverse impacts of Asian dust events on human
731 health and the environment—A probabilistic risk assessment study on particulate
732 matter-bound metals and bacteria in Seoul, South Korea, *Sci. Total Environ.*, 875,
733 162637, <https://doi.org/10.1016/j.scitotenv.2023.162637>, 2023.
- 734 Seager, R., Cane, M., Henderson, N., Lee, D., Abernathey, R., and Zhang, H.:
735 Strengthening tropical Pacific zonal sea surface temperature gradient consistent
736 with rising greenhouse gases, *Nat. Clim. Change*, 9, 517–522,
737 <https://doi.org/10.1038/s41558-019-0505-x>, 2019.
- 738 Shao, Y., Wyrwoll, K.-H., Chappell, A., Huang, J., Lin, Z., McTainsh, G. H., Mikami,
739 M., Tanaka, T. Y., Wang, X., and Yoon, S.: Dust cycle: An emerging core theme in
740 Earth system science, *Aeolian Res.*, 2, 181-204,
741 <https://doi.org/10.1016/j.aeolia.2011.02.001>, 2011.
- 742 Singh, C., Ganguly, D., and Dash, S. K.: Dust load and rainfall characteristics and their
743 relationship over the South Asian monsoon region under various warming
744 scenarios, *J. Geophys. Res. Atmos.*, 122, 7896-7921,
745 <https://doi.org/10.1002/2017JD027451>, 2017.
- 746

- 747 Su, B., Huang, J., Mondal, S. K., Zhai, J., Wang, Y., Wen, S., Gao, M., Lv, Y., Jiang, S.,
748 Jiang, T., and Li, A.: Insight from CMIP6 SSP-RCP scenarios for future drought
749 characteristics in China, *Atmos. Res.*, 250, 105375,
750 <https://doi.org/10.1016/j.atmosres.2020.105375>, 2021.
- 751 Tanaka, T. Y., and Chiba, M.: A numerical study of the contributions of dust source
752 regions to the global dust budget, *Glob. Planet. Change*, 52, 88-104,
753 <https://doi.org/10.1016/j.gloplacha.2006.02.002>, 2006.
- 754 Tegen, I., Werner, M., Harrison, S. P., and Kohfeld, K. E.: Relative importance of
755 climate and land use in determining present and future global soil dust emission,
756 *Geophys. Res. Lett.*, 31, L05105, <https://doi.org/10.1029/2003GL019216>, 2004.
- 757 van Vuuren, D. P., Stehfest, E., Gernaat, D. E., Doelman, J. C., van den Berg, M.,
758 Harmsen, M., de Boer, H. S., Bouwman, L. F., Daioglou, V., Edelenbosch, O. Y.,
759 Girod, B., Kram, T., Lassaletta, L., Lucas, P. L., van Meijl, H., Müller, C., van
760 Ruijven, B. J., van der Sluis, S., and Tabeau, A.: Energy, land-use and greenhouse
761 gas emissions trajectories under a green growth paradigm, *Global Environ.*
762 *Change*, 42, 237–250, 2017.
- 763 Wang, H., Easter, R. C., Rasch, P. J., Wang, M., Liu, X., Ghan, S. J., Qian, Y., Yoon, J.-
764 H., Ma, P.-L., and Vinoj, V.: Sensitivity of remote aerosol distributions to
765 representation of cloud–aerosol interactions in a global climate model, *Geosci.*
766 *Model Dev.*, 6, 765–782, <https://doi.org/10.5194/gmd-6-765-2013>, 2013.
- 767 Wang, P., Yang, Y., Xue, D., Ren, L., Tang, J., Leung, L. R., and Liao, H.: Aerosols
768 overtake greenhouse gases causing a warmer climate and more weather extremes
769 toward carbon neutrality, *Nat. Commun.*, 14, 7257,
770 <https://doi.org/10.1038/s41467-023-42891-2>, 2023.
- 771 Woodward, S., Roberts, D. L., and Betts, R. A.: A simulation of the effect of climate
772 change–induced desertification on mineral dust aerosol, *Geophys. Res. Lett.*, 32,
773 L18810, <https://doi.org/10.1029/2005GL023482>, 2005.
- 774 Wu, M., Liu, X., Yu, H., Wang, H., Shi, Y., Yang, K., Darmenov, A., Wu, C., Wang, Z.,
775 Luo, T., Feng, Y., and Ke, Z.: Understanding processes that control dust spatial
776 distributions with global climate models and satellite observations, *Atmos. Chem.*
777 *Phys.*, 20, 13835–13855, <https://doi.org/10.5194/acp-20-13835-2020>, 2020.
- 778 Wubben, E., Spiering, B. R., Veenstra, T., Bos, R., Wang, Z., van Dijk, J., Raffi, I.,
779 Witkowski, J., Hilgen, F. J., Peterse, F., Sangiorgi, F., and Sluijs, A.: Tropical
780 warming and intensification of the West African Monsoon during the Miocene
781 Climatic Optimum, *Paleoceanogr. Paleoclimatol.*, 39, e2023PA004767,
782 <https://doi.org/10.1029/2023PA004767>, 2024.
- 783 Xie, X., Myhre, G., Che, H., Wu, F., Guo, J., Shi, Z., Li, X., Liu, X., and Liu, Y.:
784 Anthropogenic sulfate-climate interactions suppress dust activity over East Asia,
785 *Commun. Earth Environ.*, 6, 159, <https://doi.org/10.1038/s43247-025-02147-x>,
786 2025.

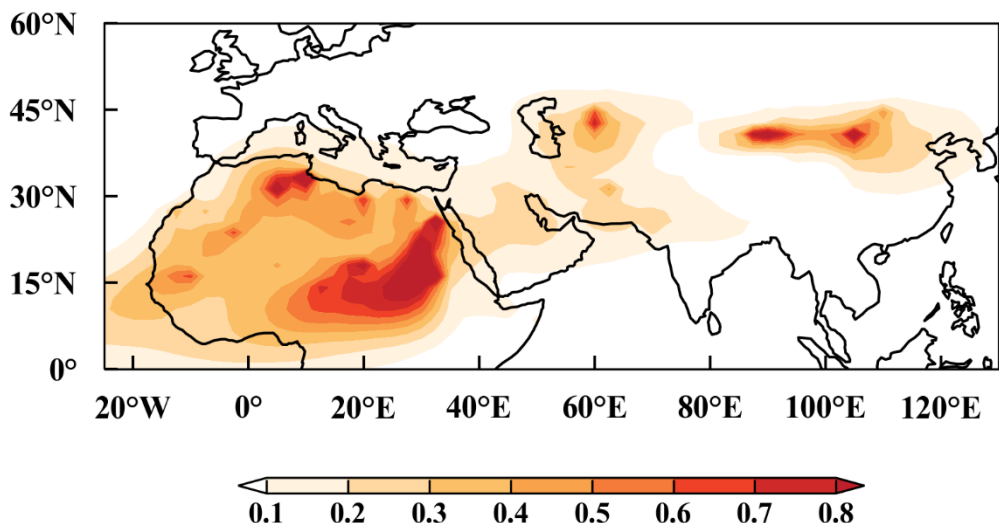
- 787 Yang, Y., Zeng, L., Wang, H., Wang, P., and Liao, H.: Climate effects of future aerosol
788 reductions for achieving carbon neutrality in China, *Sci. Bull.*, 68, 902-905,
789 <https://doi.org/10.1016/j.scib.2023.03.048>, 2023.
- 790 Yang, Y., Zeng, L., Wang, H., Wang, P., and Liao, H.: Dust pollution in China affected
791 by different spatial and temporal types of El Niño, *Atmos. Chem. Phys.*, 22,
792 14489–14502, <https://doi.org/10.5194/acp-22-14489-2022>, 2022.
- 793 Yuan, T., Huang J., Cao J., Zhang G., and Ma X.: Indian dust-rain storm: Possible
794 influences of dust ice nuclei on deep convective clouds, *Sci. Total Environ.*, 779,
795 146439, <https://doi.org/10.1016/j.scitotenv.2021.146439>, 2021.
- 796 Zender, C. S., Bian, H., and Newman, D.: Mineral Dust Entrainment and Deposition
797 (DEAD) model: Description and 1990s dust climatology, *J. Geophys. Res.*, 108,
798 4416, <https://doi.org/10.1029/2002JD002775>, D14, 2003.
- 799 Zhang, Y., Yu, F., Luo, G., Fan, J., and Liu, S.: Impacts of long-range-transported
800 mineral dust on summertime convective cloud and precipitation: a case study over
801 the Taiwan region, *Atmos. Chem. Phys.*, 21, 17433–17451,
802 <https://doi.org/10.5194/acp-21-17433-2021>, 2021.
- 803 Zhao, Y., Yue, X., Cao, Y., Zhu, J., Tian, C., Zhou, H., Chen, Y., Hu, Y., Fu, W., and
804 Zhao, X.: Multi-model ensemble projection of the global dust cycle by the end of
805 21st century using the Coupled Model Intercomparison Project version 6 data,
806 *Atmos. Chem. Phys.*, 23, 7823–7838, <https://doi.org/10.5194/acp-23-7823-2023>,
807 2023.
- 808 Zhou, Y., Wu, T., Zhou, Y., Zhang, J., Zhang, F., Su, X., Jie, W., Zhao, H., Zhang, Y.,
809 and Wang, J.: Can global warming bring more dust?, *Clim. Dyn.*, 61, 2693–2715,
810 <https://doi.org/10.1007/s00382-023-06706-w>, 2023.
- 811 Zhu, J., Yang, Y., Wang, H., Gao, J., Liu, C., Wang, P., and Liao, H.: Impacts of
812 projected changes in sea surface temperature on ozone pollution in China toward
813 carbon neutrality, *Sci. Total Environ.*, 915, 170024,
814 <https://doi.org/10.1016/j.scitotenv.2024.170024>, 2024.
- 815



816
817 **Figure 1.** Seasonal mean (a) dust near-surface concentration ($\mu\text{g m}^{-3}$) and (b) dust
818 emission ($\text{kg m}^{-2} \text{s}^{-1}$) during boreal spring (March-April-May), summer (June-July-
819 August), Autumn (September-October-November) and winter (December-January-
820 February) of 2060 over the dust belt (0° – 60°N , 25°W – 130°E) simulated from the
821 Fut_CNeutral, Fut_SSP585, AA_CNeutral and GHG_CNeutral simulations.
822

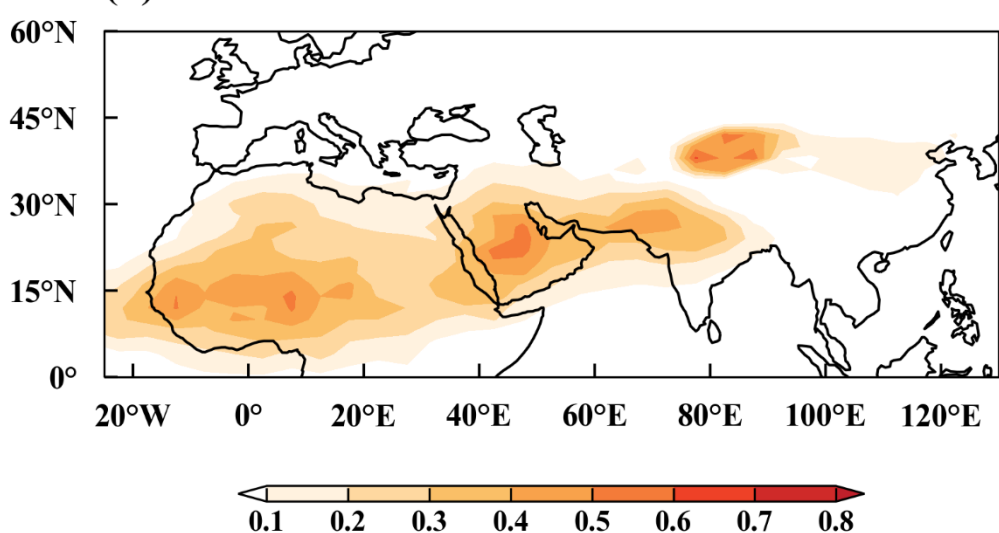
823 (a) CESM

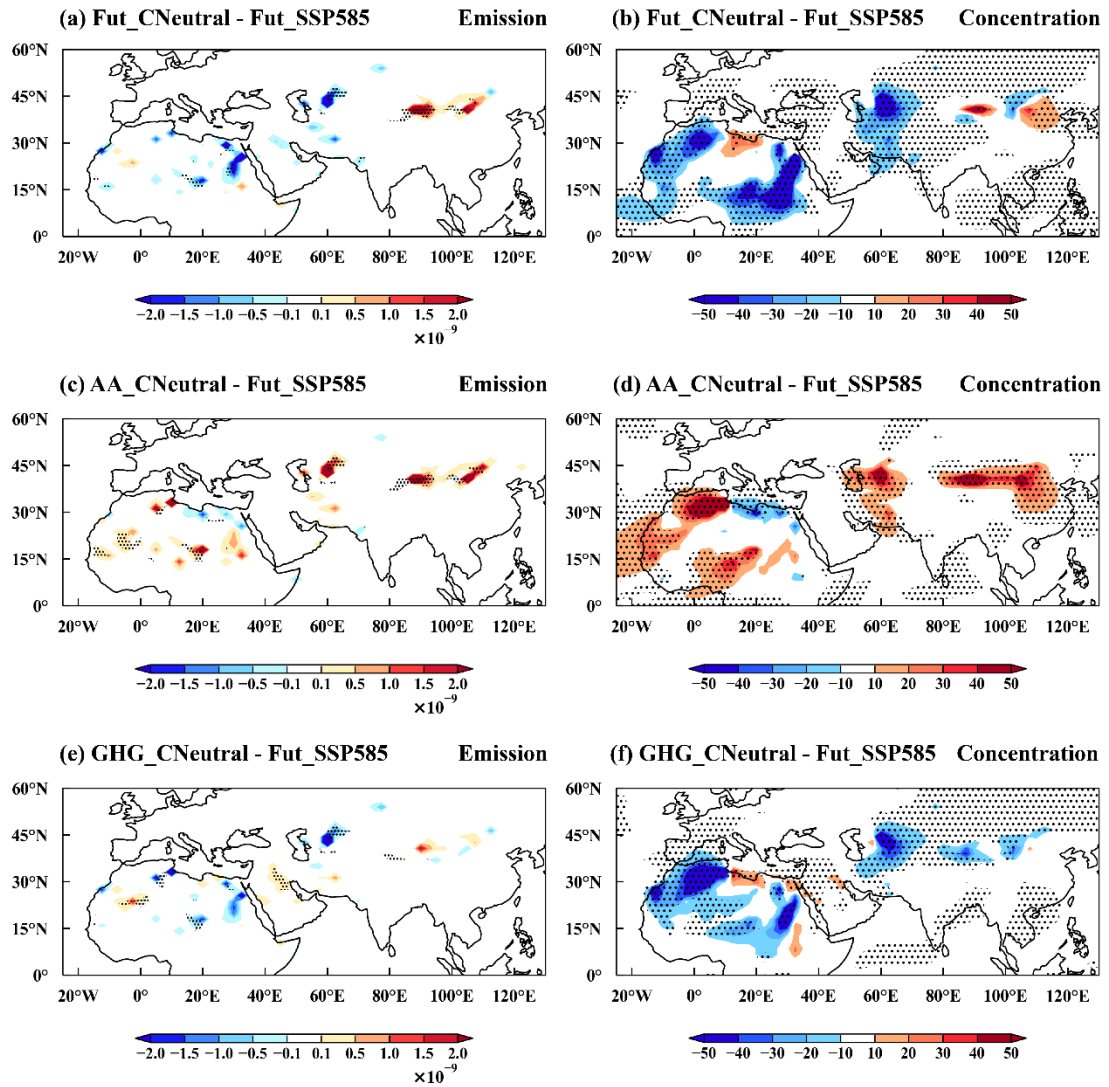
824 3-5



828 (b) CALIPSO

829 3-5



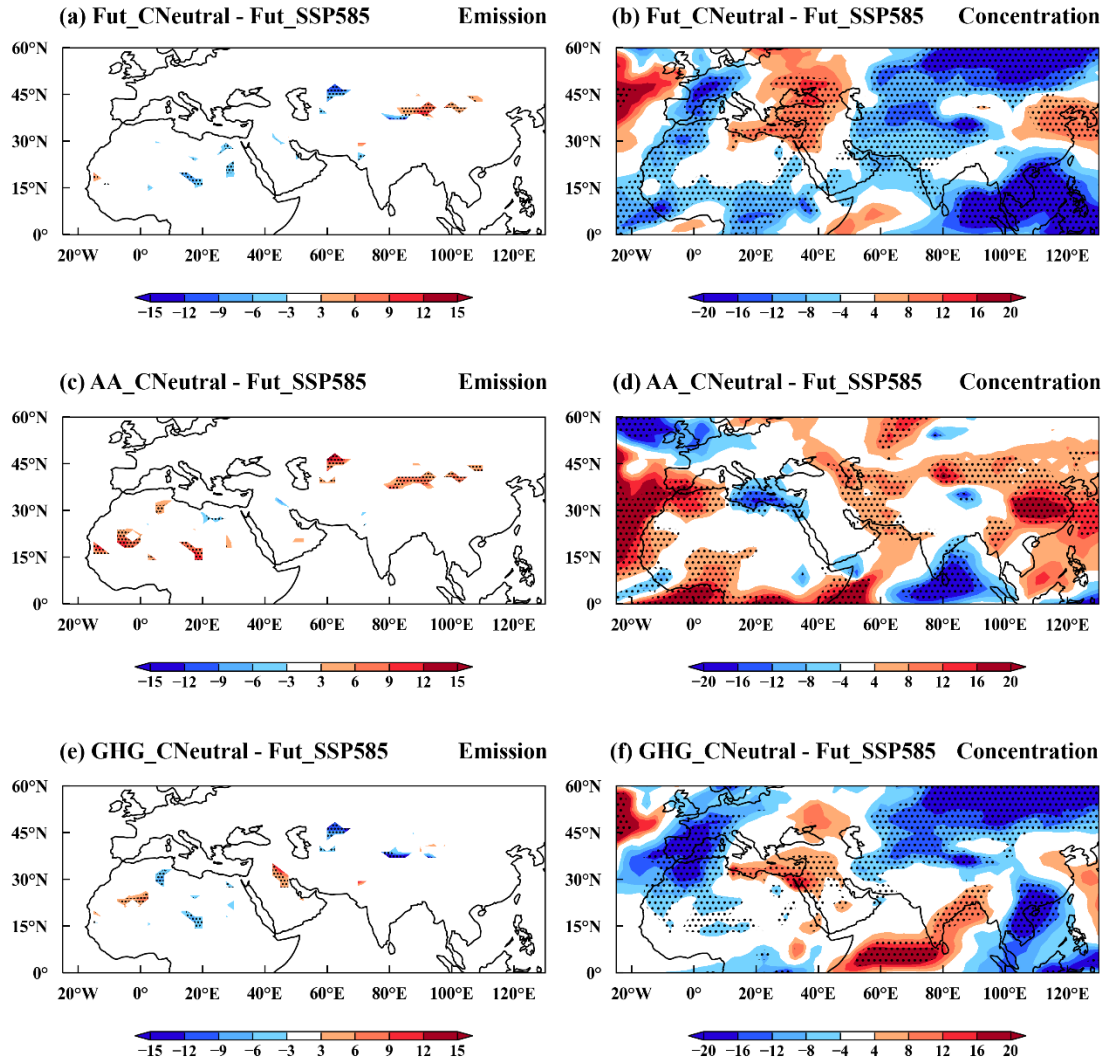


828

829 **Figure 3.** Spatial distribution of changes in March–May mean (a, c, e) dust emissions
 830 ($\text{kg m}^{-2} \text{ s}^{-1}$) and (b, d, f) near-surface dust concentrations ($\mu\text{g m}^{-3}$) in 2060 for
 831 Fut_CNeutral (top), AA_CNeutral (middle), and GHG_CNeutral (bottom) compared to
 832 the Fut_SSP585 simulation. The stippled areas indicate statistically significant
 833 differences at the 90% confidence level based on a two-tailed Student's t test.

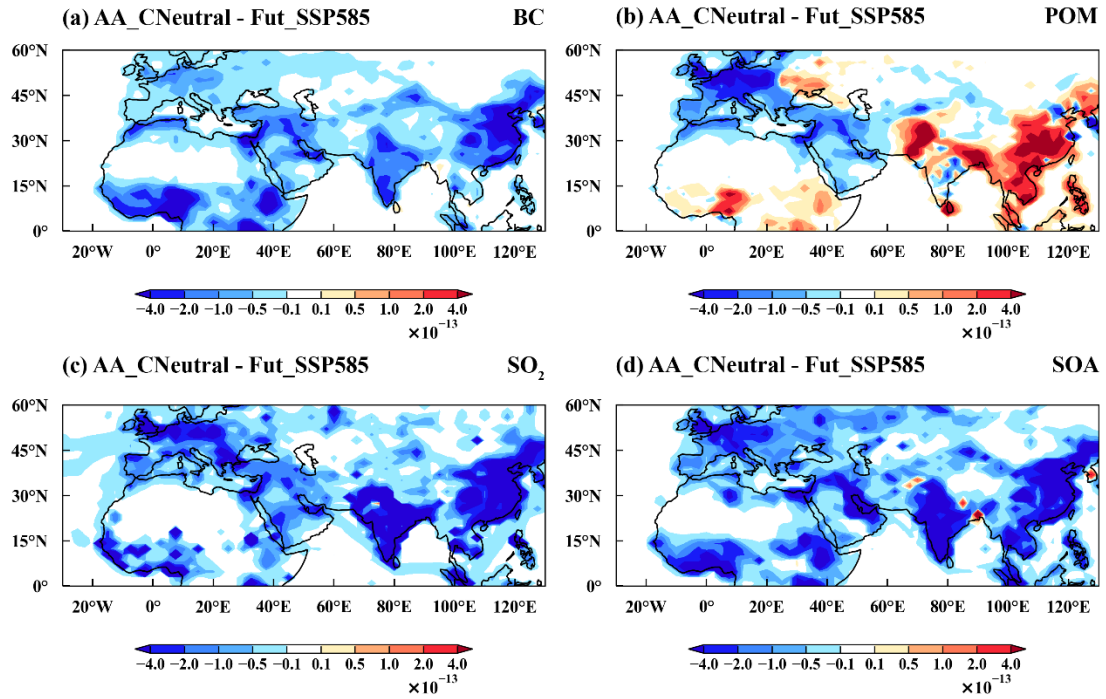
834

835



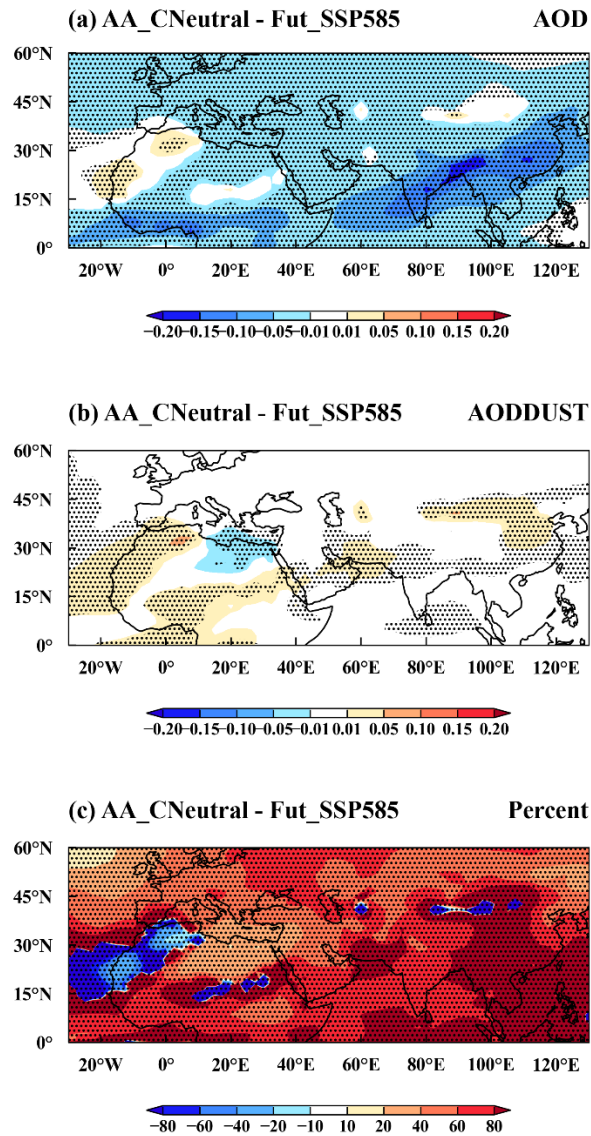
836

837 **Figure 4.** Spatial distribution of percentage changes in March–May mean (a, c, e) dust
 838 emissions (%) and (b, d, f) near-surface dust concentrations (%) in 2060 for
 839 Fut_CNeutral (top), AA_CNeutral (middle), and GHG_CNeutral (bottom) compared to
 840 the Fut_SSP585 simulation. The stippled areas indicate statistically significant
 841 differences at the 90% confidence level based on a two-tailed Student's t-test.
 842

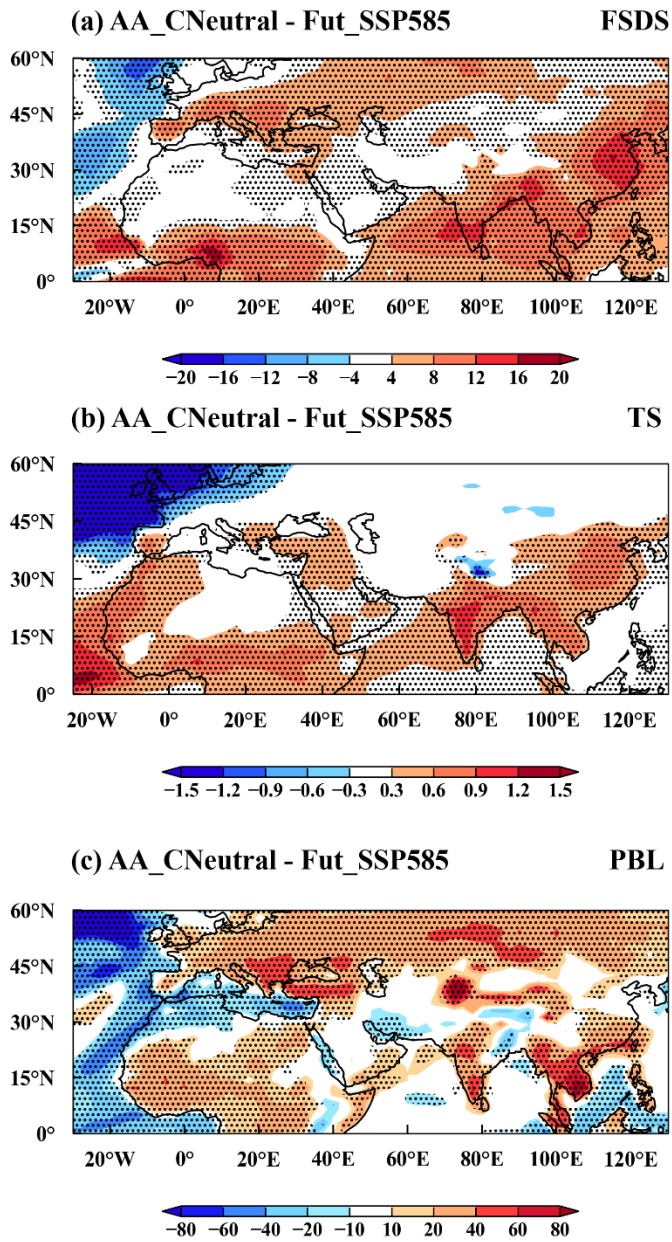


843
844 **Figure 5.** Spatial distribution of changes in March–May mean (a) black carbon (BC,
845 kg m⁻² s⁻¹), (b) particulate organic matter (POM, kg m⁻² s⁻¹), (c) sulfur dioxide (SO₂, kg
846 m⁻² s⁻¹), and (d) precursor gas of secondary organic aerosol (SOAG, Tg m⁻² yr⁻¹) in 2060
847 for AA_CNeutral, compared to the Fut_SSP585 simulation.

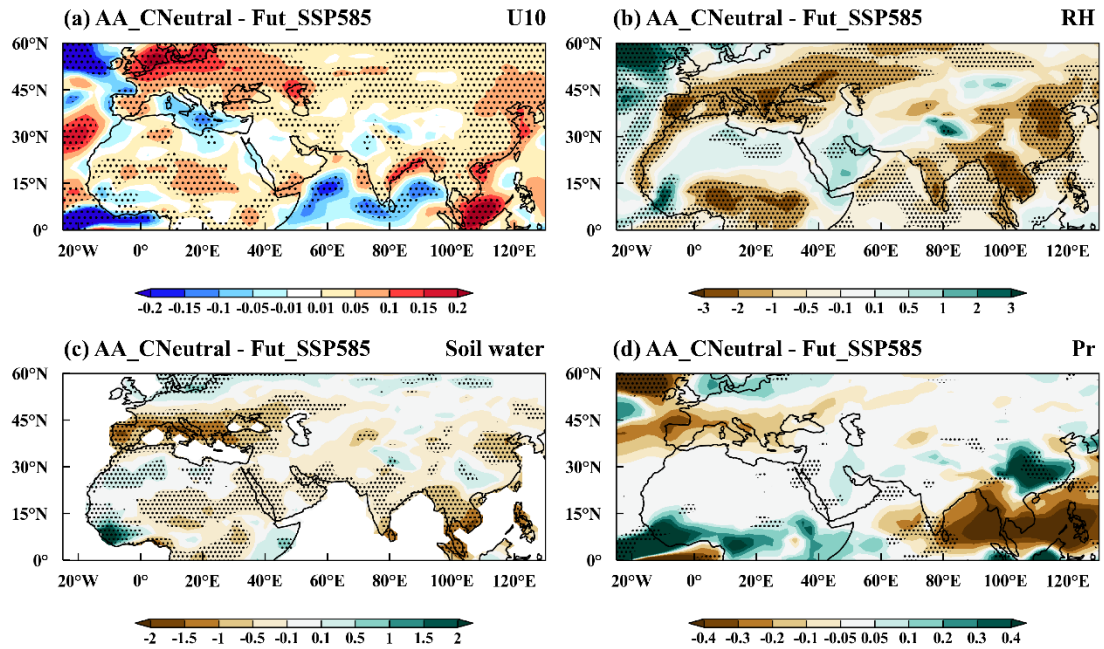
848
849



850
851 **Figure 6.** Spatial distribution of changes in March–May mean (a) aerosol optical depth
852 (AOD), (b) aerosol optical depth from dust (AODDUST), and (c) the fraction of sulfate
853 AOD change in total AOD change (%) in 2060 for AA_CNeutral, compared to the
854 Fut_SSP585 simulation.
855



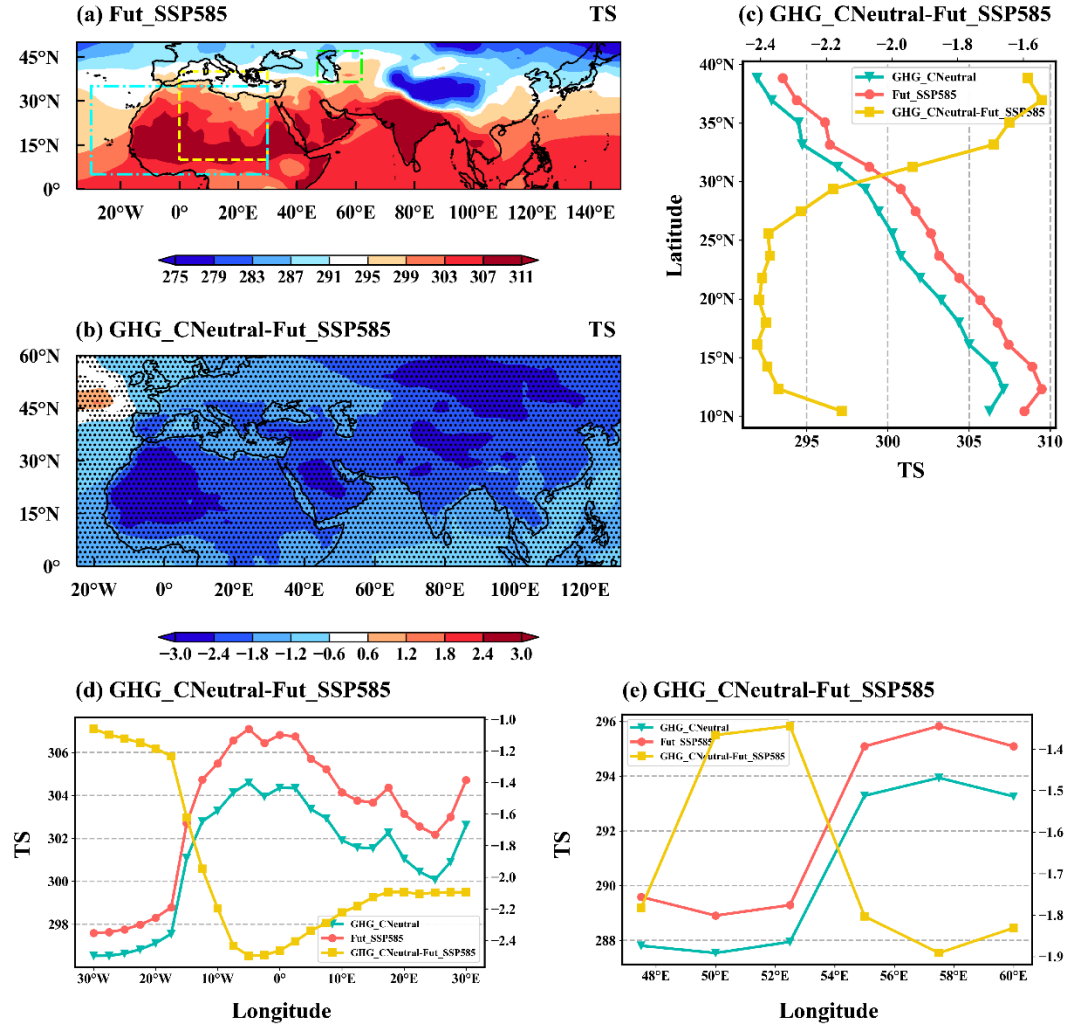
856
 857 **Figure 7.** Spatial distribution of changes in March–May mean (a) downwelling solar
 858 flux at the surface (FSDS, W/m^2), (b) surface temperature (TS, K), and (c) planetary
 859 boundary layer height (PBL, m), in 2060 for AA_CNeural, compared to the
 860 Fut_SSP585 simulation. The stippled areas indicate statistically significant differences
 861 at the 90% confidence level based on a two-tailed Student's t test.



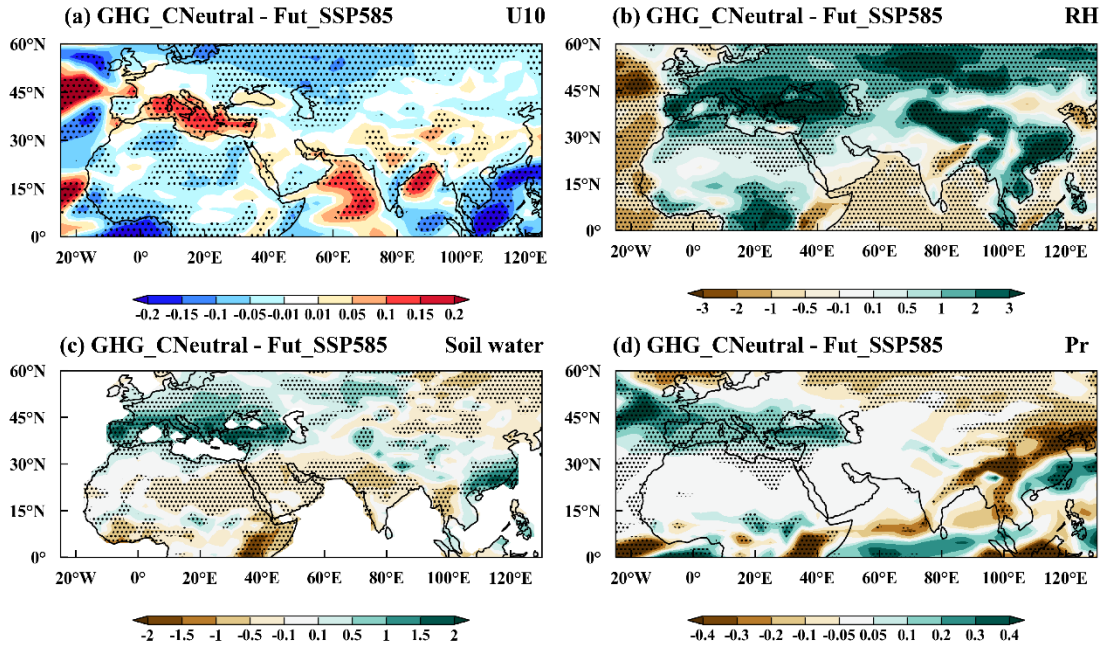
863

864 **Figure 8.** Spatial distribution of changes in March–May mean (a) 10-meter wind speed
 865 (U10, m s^{-1}), (b) relative humidity (RH, %), (c) soil water content (soil water, kg m^{-2}),
 866 and (d) precipitation rate (pr, mm day^{-1}) in 2060 for AA_CNeutral, compared to the
 867 Fut_SSP585 simulation. The stippled areas indicate statistically significant differences
 868 at the 90% confidence level based on a two-tailed Student's t test.

869

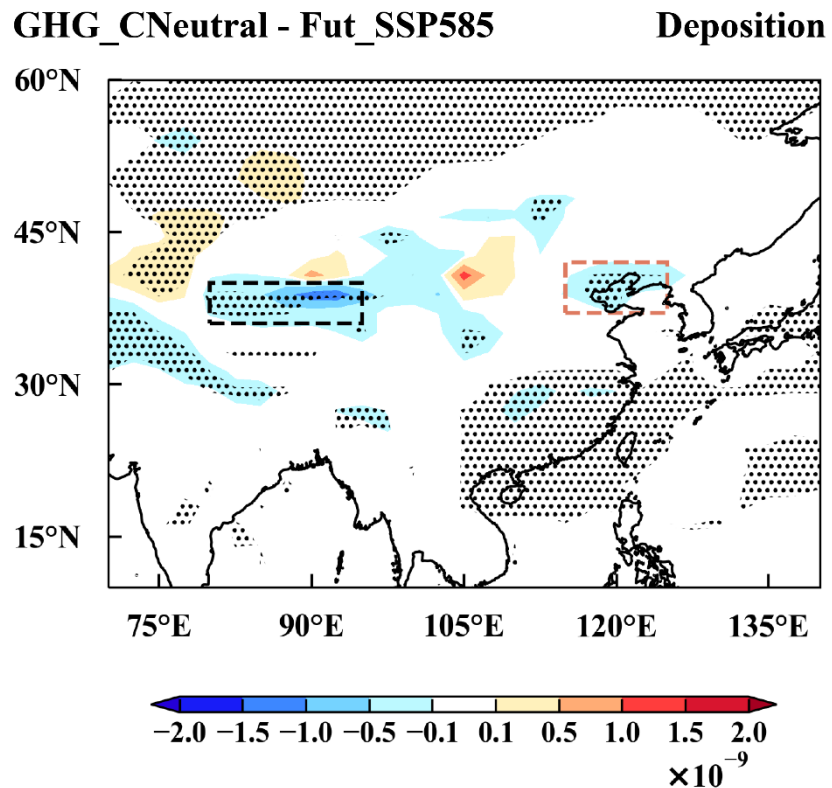


870
871 **Figure 9.** Spatial distribution of March–May mean (a) surface temperature (TS, K) in
872 2060 from Fut_SSP585 and (b) changes in March–May mean surface temperature (TS, K)
873 in 2060 for GHG_CNeutral, compared to the Fut_SSP585 simulation. The stippled
874 areas in (a) and (b) indicate statistically significant differences at the 90% confidence
875 level based on a two-tailed Student's t test. (c) Zonal averaged TS (K) over the region
876 (10°–40°N, 0°–30°E, yellow) and (d–e) meridional averaged TS (K) over the regions
877 (5°–35°N, 30°W–30°E, blue; 36.5°–47°N, 47°–62°E, green) marked in (a) from March
878 to May in 2060 for GHG_CNeutral, Fut_SSP5-8.5, and the changes between
879 GHG_CNeutral and Fut_SSP5-8.5.
880

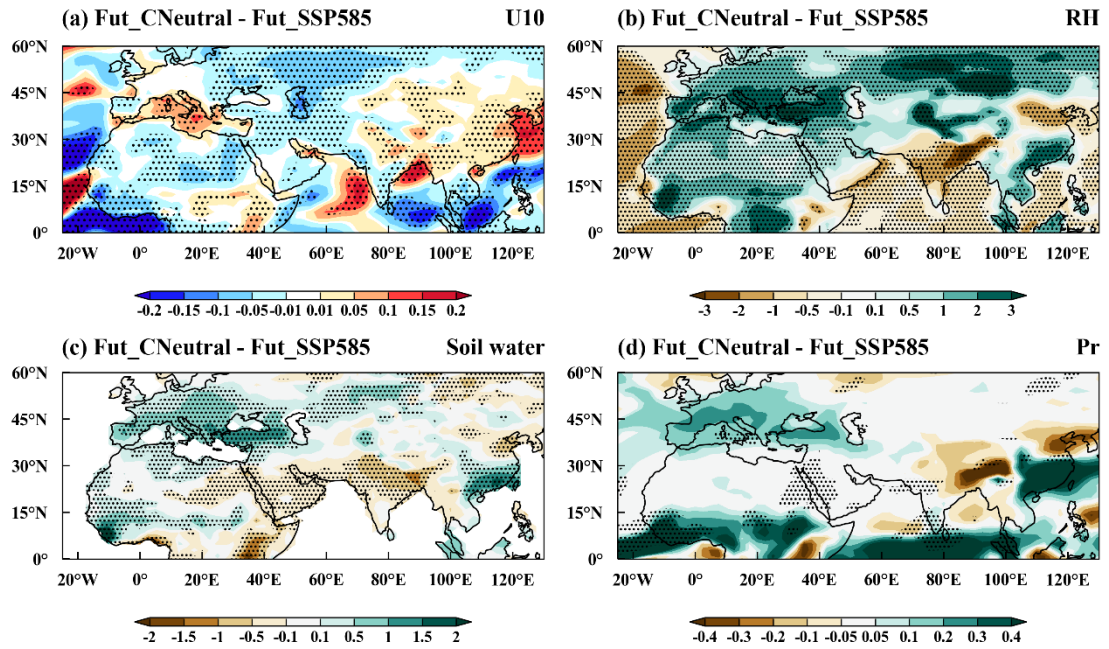


881

882 **Figure 10.** Spatial distribution of changes in March–May mean (a) 10-meter wind
 883 speed (U10, m s^{-1}), (b) relative humidity (RH, %), (c) soil water content (soil water, kg m^{-2}),
 884 and (d) precipitation rate (pr, mm day^{-1}) in 2060 for GHG_CNeutral, compared to
 885 the Fut_SSP585 simulation. The stippled areas indicate statistically significant
 886 differences at the 90% confidence level based on a two-tailed Student's t test.
 887



888
 889 **Figure 11.** Spatial distribution of dust deposition ($\text{kg m}^{-2} \text{ s}^{-1}$) changes for the period of
 890 March to May in 2060 between GHG_CNeutral and Fut_SSP585 scenarios. The stippled
 891 areas indicate statistically significant differences at the 90% confidence level based on
 892 a two-tailed Student's t test. Negative values denote more dust deposition to the surface.
 893 The Taklimakan (black box) and North China Plain (brown box) are highlighted.
 894
 895



896

897 **Figure 12.** Spatial distribution of changes in March–May mean (a) 10-meter wind
 898 speed (U10, m s^{-1}), (b) relative humidity (RH, %), (c) soil water content (soil water, kg m^{-2}),
 899 and (d) precipitation rate (pr, mm day^{-1}) in 2060 for *Fut_CNeutral*, compared to
 900 the *Fut_SSP585* simulation. The stippled areas indicate statistically significant
 901 differences at the 90% confidence level based on a two-tailed Student's t test.

902

903

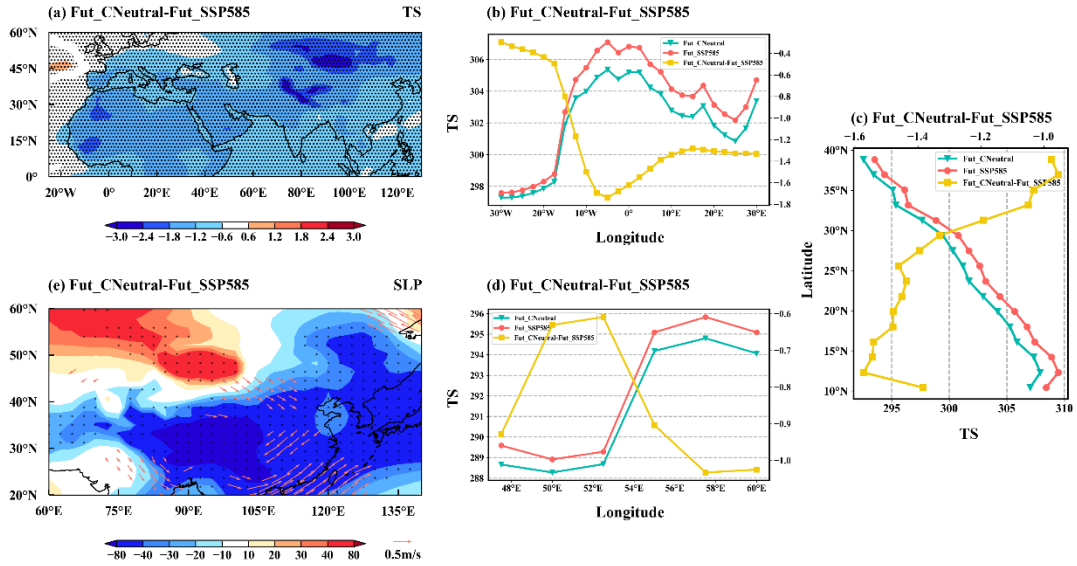


Figure 13. Spatial distribution of changes in March–May mean (a) surface temperature (TS, K) and (e) sea level pressure (SLP, Pa) in 2060 for *Fut_CNeutral*, compared to the *Fut_SSP585* simulation. The stippled areas in (a) and (b) indicate statistically significant differences at the 90% confidence level based on a two-tailed Student's t test. (c) Zonal averaged TS (K) over the region (10° – 40° N, 0° – 30° E) and (b, d) meridional averaged TS (K) over the regions (5° – 35° N, 30° W– 30° E; 36.5° – 47° N, 47° – 62° E) marked in (a) from March to May in 2060 for *Fut_CNeutral*, *Fut_SSP5-8.5*, and the changes between *Fut_CNeutral* and *Fut_SSP5-8.5*.

904

905

906

907

908

909

910

911

912

913